Tunneling Current and Topographical Measurements of Semiconducting Structures Relevant for Electronic Applications using Atomic Force Microscopy

by

Benjamin Vaughn Schoenek

A thesis submitted to the Graduate Faculty of
Auburn University
in partial fulfillment of the
requirements for the Degree of
Master of Science

Auburn, Alabama
August 5, 2017

Keywords: AFM, SiC, BSG, I-AFM, WSe2, Peizoresistive

Approved by

Dr. Sarit Dhar, Chair, Associate Professor of Physics
Dr. Marcelo Kuroda, CoChair, Assistant Professor of Physics
Dr. Minseo Park, Professor of Physics

Abstract

This thesis is a combination of a synopsis of techniques used in Atomic Force Microscopy and its subsidiary uses as well as a record of experimental data taken using the instrument for two separate experiments. The first experiment shows the relationship between tunneling current and force applied by the Atomic Force Microscope (AFM) on two dimensional WSe_2. This experiment is based on a previous experiment on single layer MoS_2. The second experiment shows changes in the layer thickness of Boro-Silicate Glass (BSG) thin films due to different annealing conditions. These experiments focus on the application of I-AFM (the I stands for current) and Non-Contact Atomic Force Microscopy (NC-AFM) in the characterization and exploration of structural and electrical characteristics for use of these materials in electronic applications. The application of the AFM in these experiments, amongst other tasks not included in this thesis, allowed the author to reach a deep understanding of AFM.

Acknowledgments

There were many individuals who contributed to the experiments and also my own wellbeing during this process. This list may be incomplete, but I did my best to remember all who contributed.

Dr. Sarit Dhar, Dr. Marcelo Kuroda, Dr. Minseo Park, Dr. Hui Zhao, Asanka L. Jayawardena, Yongju Zheng, Isanka Jayawardhena, Dr. Ayahi (Claude) Ahyi, Tamara Issacs-Smith, and my friends and family.

Table of Contents

List of Figures

List of Tables

Chapter 1

Introduction

Electronic applications of semiconducting materials has, and continues to be, a large motivation for exploring the physics behind their functionality. Development in this area also helps increase the rate at which these materials are studied, since their application in computational and experimental devices is extensive. At the heart of these devices is the transistor; effectively an on/off switch that allows basic logic to be performed in a rapid manner. The push for faster, energy efficient, and more powerful devices has led to smaller and smaller transistors, hence the familiar mentioning of Moore's law in recent scientific literature [2]. Advancement in the application, design, and understanding of such devices requires a push in the physical understanding of these devices. The materials used to make these devices functional, their atomic structure, quantum effects, electrical characteristics et cetera rely on the understanding and combining of many physical principles from all different theories and branches of physics.

1.1 Atomic Force Microscopy

To design and characterize new devices and novel materials, different techniques need to be employed. Electrical characterization, imaging, and fabrication techniques all contribute to understanding these devices. Atomic Force Microscopy (AFM) is one of these techniques, designed to explore topography and electrical characteristics. Its use in the larger scope of semiconducting technology is a major focus of this thesis.

The initial motivation for the development of these characterization techniques was to image individual atoms. This was achieved in 1981 with the introduction of the Scanning

Tunneling Microscope (STM) by Binning, Rhorer, Gerber, and Weibel. Binnig et al. successfully imaged the Si 111 structure in 1983. Despite the success of the STM, the technique is limited to conducting samples. The STM uses tunneling electrons to create the image, therefore conduction from the tip, through the sample, and into the stage is required. This led to the creation of the AFM. The first AFM was created by Binnig, Quate, and Gerber in 1986 [3]. The technique requires no vacuum and can image any unprepared surface at room temperature, while still showing near atomic scale resolution.

Since its creation, AFM is now used extensively for device imaging and characterization. Different modes have been added to allow even more functionality from the technique, such as electrical characterization. Although STM has better resolution, AFM has its own unique skill set. These imaging techniques are now widely used by the scientific and industrial community due to their usefulness in helping researchers develop new devices.

What makes the AFM so simple and able to work with such high resolution at room temperature and atmospheric conditions is that the AFM works with the principle of force. The AFM keeps a constant force on a surface, and recording the movements necessary to keep that force constant will generate an image. More details about how this works will be covered in Chapter 2, along with the different applications and modes for the AFM. To measure the force, something needs to contact the sample, although once again another technique called Non-Contact AFM gets around this limitation but will be covered later. Generally an AFM uses a cantilever to contact the sample. This is a small, flexible arm that is generally made of silicon. Due to the flexibility of the cantilever a basic spring force equation can be used to model the system. For a cantilever with width w, length L, and thickness t the spring constant is given by [3]:

$$k = \frac{Ywt^3}{4L^3} \tag{1.1}$$

Y is Young's modulus, a constant based on the material used to make the cantilever. Other forces interact with the AFM tip as it takes an image, but the simplicity of the method remains, and allows it to function in ways other characterization techniques cannot.

1.2 TMD's

The relatively recent discovery of exfoliation techniques for creating single layer Transition Metal Dichalcogenides (TMD's) and other two dimensional materials has significantly reinvigorated and given a new direction in the study of these materials for use in electronic devices. Before it was difficult and expensive to isolate thin layers of these materials for study. This new nobel-prize winning technique demonstrated on graphite, known as the scotch tape method, has made this process cheap and therefore lucrative for study [5]. TMD's have a MX_2 structure where the M is a transition metal (Mo, W, Re, Nb, etc) and the X is a chalcogen atom (S, Se, or Te) [4]. Due to their atomic structure, the properties of these materials not only differ from the bulk material in the thin layered form, but can also be manipulated to exhibit a full range of electrical characteristics, different from the bulk, useful for nano-electronic devices. In chapter 3, AFM will be used to characterize these materials and explore vertical charge transport and tunneling as it relates to pressure in WSe_2. Understanding the properties of these materials will allow new ways to use them in electronic devices.

1.3 SiC and MOSFET Technology

One common design for a transistor is the Field Effect Transistor (FET). A field effect transistor uses an electric field to allow the flow of electrons through the device, allowing the on/off switching functionality required of a transistor. When the device is made from the combination of a metal, oxide, and semiconductor the device is described as a Metal-Oxide-Semiconductor Field Effect Transistor (MOSFET) (see Figure 1.1). Regions in the

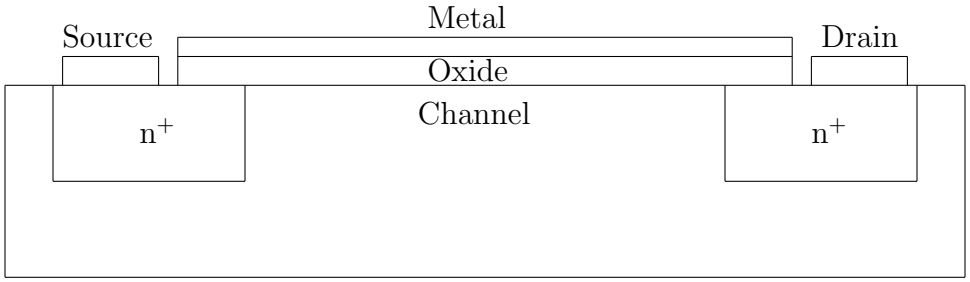

Figure 1.1: A MOSFET is a field effect transistor composed of a metal, oxide, and semiconductor. Source, drain, and Gate are composed of the metal. The semiconductor forms the main structure of the device and the oxide forms a barrier between the channel and the metal gate.

semiconductor are doped with other elements to allow for excess electrons in the semiconductor, allowing conduction through the device. As bias is applied to the gate, the electric field generated in the channel region lowers the potential barrier between the doped regions, allowing current to flow.

What is important for the functionality of these devices is the interaction of the particular materials used for the metal, oxide, and semiconductor. Generally silicon is used as the semiconductor and is in the majority of devices in electronics used today, however, as mentioned previously, there are many materials for advance electronics. For example, silicon carbide, a material studied extensively by the authors research group, is used in high power devices due to it's thermal properties and higher band gap (3.2 eV). In chapter 4 the AFM will be used to characterize thin Boro-Silicate Glass films for use in MOSFETs. BSG shows promising mobility characteristics, however it suffers from instability issues with applied bias. In an attempt to reduce the effects of the instability in BSG, thin films are created for use with SiO_2, a more stable, but unfavorable oxide due to higher trap density, leading to lower mobility in devices.

Chapter 2

Atomic Force Microscopy Methods

2.1 Park Systems XE7 Atomic Force Microscope

The Atomic Force Microscope (AFM) used by the author is a Park Systems XE7 system. This system allows, through the use of modules and removable portions of the microscope, multiple functions from the same basic framework. The device consists of an ocular microscope attached above a modular AFM. The optical microscope allows real time optical imaging of the sample. Additionally, it allows optical alignment of the laser used in the system as well as optical diagnostics of the particular AFM tip being used for the particular experiment.

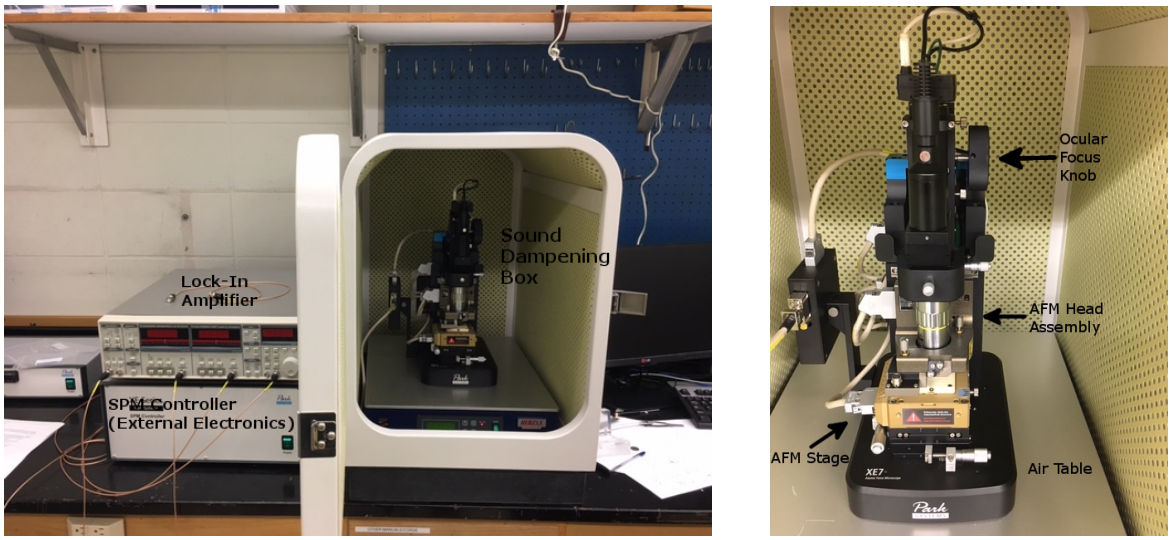

Figure 2.1: Park Systems XE7 Atomic Force Microscope: right image is entire system as described, left image is closeup on AFM.

To reduce vibrational noise from the external environment the device is placed on an air isolation table which is housed with the microscope in a sound dampening box. The

box also rests on a concrete block. The electronics required to monitor and manipulate the delicate electronics of the microscope are housed outside of the sound dampening box. The entire device is then run via a desktop computer using software provided by Park Systems (see Figure 2.1).

2.2 Contact Atomic Force Microscopy (C-AFM)

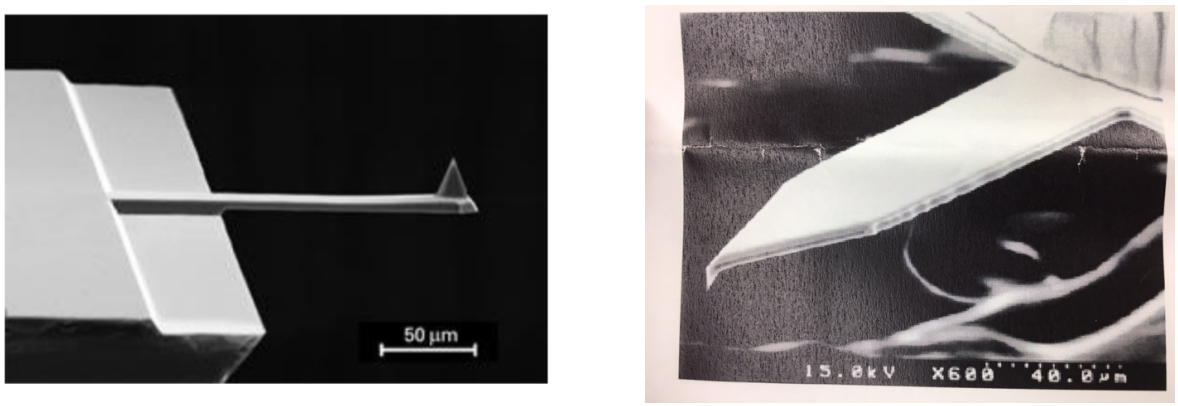

Figure 2.2: Scanning Electron Microscopy (SEM) images of AFM cantilevers. Right image is of a silicon based contact cantilever (fig. 3-2 p.43 [12]), left is of a silicon based non-contact cantilever (Data sheet for OMCL-AC160TS NC-AFM Cantilever, Park Systems)

The basics of Atomic Force Microscopy are explained by the most basic functionality of the AFM, Contact Atomic Force Microscopy (C-AFM). This is the earliest application for AFM as well as the building block for all of the other functionality of the microscope. The principle aims to image a surface at the nanoscale level by maintaining a constant force on a, generally silicon based, flexible cantilever (see Figure 2.2). A laser is used to measure the force the sample exerts back on the cantilever. The laser is bounced off the back of the cantilever, and is directed to a Charged Coupled Device (CCD). The CCD measures intensity and wavelength of the laser as the cantilever flexes under pressure applied to the cantilever by the sample (see Figure 2.3). The microscope corrects based on this applied pressure, seeking to maintain a constant force. The result is a two-dimensional topographical image of the surface. The cantilever scans in lines over the sample one at at time, recording the

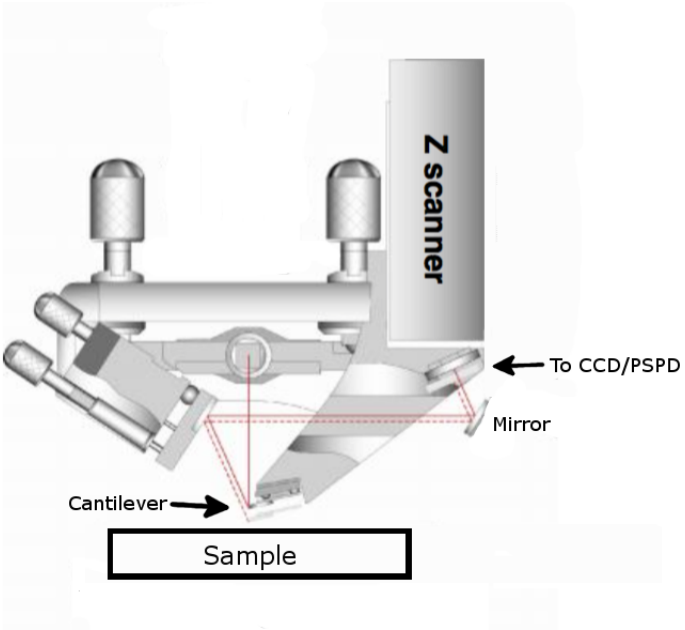

Figure 2.3: Figure depicting the path of the laser through the AFM head allowing measurement of force on the cantilever for topographical measurements [12].

height adjustments made by the microscope. To keep the force constant on the cantilever as it scans the surface requires real time adjustment. This is accomplished by the external electronics of the AFM, which effectively create a feedback loop with the cantilever, the laser, and the external electronics. By keeping track of the vertical adjustments required to maintain the force on the sample an image is generated.

C-AFM allows imaging of atomic layers in some films since the method can distinguish sub nanometer level topographical changes of surface structures. Using this technique the author achieved nanometer level measurements with the device to characterize and determine roughness to nanometer levels of precision in various experiments. The AFM would measure smaller changes in topography, however there is a limitation to the technique. The physical limitation, simply put, is the material the cantilever is made of, not specifically which element it is composed of, but rather that it is made of atoms itself. AFM tip manufacturers can manufacture the tip to roughly one or two atoms at the sharpest point, however, this is

where the limitation arrises. Imaging atoms with atoms means the resolution of the image cannot be less than an angstrom.

When the AFM is set to use C-AFM the tip actually contacts the sample. This will eventually damage or wear down the cantilever tip. The tip can also pick up particles which will distort the image, causing faster degradation and generate artifacts in AFM images. The tip also runs a high risk of breaking especially on surfaces with large sudden changes in topography. These sharp changes in topography can catch the feedback loop off guard and cause the tip to crash into the sample, breaking or chipping the tip. Additionally, lateral forces are experienced by the tip as it is sometimes dragged across the sample surface. This becomes particularly relevant if the surface being scanned is soft, which allows the tip to dig into the sample leading to a tip breaking or material accumulating on the tip, distorting the image.

2.3 Artifacts in AFM Images

Due to the nature of imaging at such a small scale, especially with a method that depends on measuring force, an AFM operator must be aware of some of the instrumental errors that can arise when taking an AFM image. These artificial topographical discrepancies tend to look like real features. These false readings are called artifacts. As a result it is imperative for an AFM operator to question the quality of an image and take repeated measurements to check for inconsistency. There are many different types of artifacts, but here are some of the most common and most easily recognizable.

Figure 2.4 shows some early scans done by the author to learn about scan characteristics. The top and middle left images show a similar, but inverted pattern from the Park Systems test sample. The Park Systems test sample consists of several regions, each with a consistent repeating pattern. This particular sample has trenches, circular holes, raised circular structures, and raised square structures. Each of the dots in the top left image, or holes in the case of the middle left image, should be perfect circles (see figure 2.4). What is

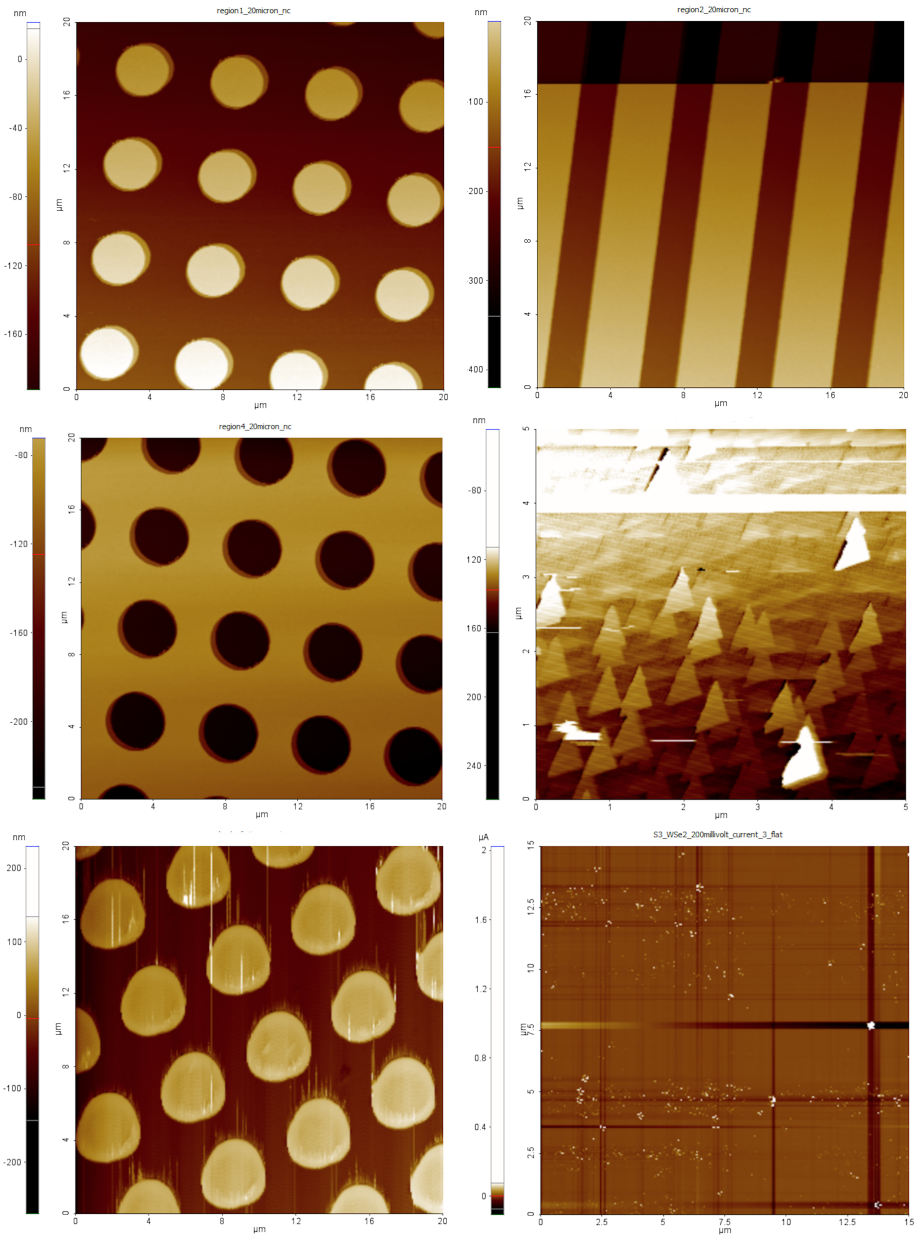

Figure 2.4: Artifacts in AFM images: Top Left: 20x20 μm C-AFM image on standard sample showing shadowing in raised features Top Right: 20x20 μm C-AFM image on standard sample showing dust grain Middle Left: 20x20 μm C-AFM image on standard sample also showing shadowing in pits Middle Right: C-AFM image 5x5 μm Ga_2O_3 image showing tip artifacts Bottom Left: 20x20 μm C-AFM image standard sample showing elongation of the same circular features in the top and middle right images due to defective AFM tip Bottom Right: 5x5 μm Flattened I-AFM Current map showing line artifacts from flattening process

shown in the image is a shadowing effect around each of the features. This artifact is due to the stage of the AFM not being able to react to the changes in topography quick enough.

In this case, as the cantilever passes over the circle it has a delay in recognizing the sudden drop off from each feature. This generates the shadow, which to the AFM seems to be a real topographical feature. This feature is not seen as the tip scans back over the feature, going from lower to higher elevation. To verify this is an artifact the AFM operator simply needs to take a secondary scan of the same spot on the sample after rotating the sample, or changing the direction of the scan. The shadowing effect will rotate around the features based on the scan direction.

In the top right image of figure 2.4 there is a dark region towards the top of the image. Since color corresponds to a difference in topography, this would seem to be a real topographical change on the sample. Upon closer inspection it is noticed that a small white (in the case of this image) dot is seen at the boundary of this darker region. This dot is a dust particle that landed on the sample and due to its presence there is an artifact in the AFM image. The dust in this case is several μm in diameter and the ribbing pattern from the standard sample is around 200 nm in height. Upon detecting the dust particle, the AFM notices a large change in topography and has to reset its scaling for the scan, leading to the artifact.

In the middle right image of Fig 2.4 the AFM image generated shows triangular structures. What should be noticed is the triangular structures all point in the same direction. Upon re-scanning the sample, which was expected to be very smooth, the triangles change direction and point in the direction of the scan. The artifact here is an image of the C-AFM tip, which is triangular, showing up as an artifact due to the topographical features of the sample being smaller than the tip.

Other artifacts can also be seen in AFM images. External vibrations felt by the AFM can show a repeating wave pattern on the surface, chipped tips will show false topography and elongation of surface features (see Fig 2.4 bottom left), dragging tips along the surface will also distort topographical features, and image processing, for example image flattening

(see Fig 2.4 bottom right), can lead to false lines in the final AFM image [11]. An AFM operator must be aware of the existence of artifacts to give reliable data.

2.4 Non-Contact Atomic Force Microscopy (NC-AFM)

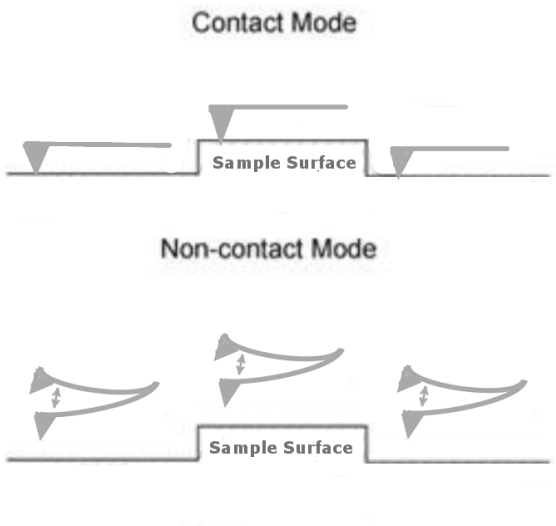

Figure 2.5: Figure showing C-AFM vs NC-AFM

To solve some of the weaknesses of C-AFM, Non-Contact AFM can be used. NC-AFM uses the same ideas and principles as C-AFM, however, as the name suggests the topographical image is generated without contacting the sample (see Figure 2.5). This is made possible by vibrating the tip above the sample during the scan rather than dragging the tip directly across the sample surface. The electrostatic and surface interaction forces from the sample are enough to attract the tip vibrating above the sample, effecting the amplitude at which it vibrates. Topography can be measured by scanning over an area while the feedback loop of the AFM adjusts the distance above the sample in an attempt to keep the amplitude of the cantilever constant. This can also be achieved similarly by tapping the tip on the sample surface, more commonly referred to at tapping AFM. The XE7 uses the former method. The advantages gained in this mode are: lower chance of tip breakdown, lower chance of attraction of particles on the tip, the ability to scan amorphous or soft

samples, and no lateral force applied to the tip while undergoing a scan. The sub nanometer resolution, in the authors experience, is generally the same as C-AFM. Additionally, NC-AFM generally leads to less artifacts in the images on very smooth samples such as bare silicon carbide.

2.5 Electrical Properties Using C-AFM

By making the AFM tip out of a conductive material such as gold or platinum additional functionality can be achieved with C-AFM. The tip can be used to measure electrical properties of the sample. The XE7 microscope can measure changes in capacitance, map potential over an area with an applied bias to the sample, map current over an area, and take IV measurements at specified points on the sample. In order, these functionalities are called Scanning Capacitance Microscopy (SCM), Electric Force Microscopy (EFM), and Current Atomic Force Microscopy (I-AFM).

2.5.1 Scanning Capacitance Microscopy (SCM)

Using the conductive C-AFM tip, it is possible to use the AFM to measure the differential capacitance $\frac{\partial C}{\partial V}$ over a sample. Bias is applied to the sample stage and the bias is measured by the tip as it passes over the sample. Due to the signal to noise ratio of such a measurement, the use of a lock-in amplifier is required. A lock-in amplifier drives a waveform that is monitored and changed by the operator to amplify the signal from the SCM making it larger and therefore separate from the background noise. To find the overall capacitance of a sample it is necessary to integrate the $\frac{\partial C}{\partial V}$ over the scan area.

2.5.2 Electric Force Microscopy (EFM)

Similar to SCM this type of measurement is done to map out the differences in electrical characteristics of the sample by applying a bias to the sample and measuring the output bias with the AFM tip. This process does not require a lock-in amplifier, although if a lock-in

amplifier is used as a replacement for the AFM's internal electronics, which is sometimes preferable, the method is called EXT-EFM.

2.5.3 Current Atomic Force Microscopy (I-AFM)

This method measures current using the conductive AFM tip. The method measures differences in the current carrying properties of the material in a topological scan. Once the scan is achieved the tip can also be positioned at a singular point on the sample and used to take an IV sweep. This procedure was heavily utilized in attempts to determine tunneling currents in the WSe_2 and WS_2 flakes.

Chapter 3

Tunneling Measurements in WSe2 Using I-AFM

3.1 Motivation for Experiment

Using I-AFM, it has been reported that it is possible to study vertical charge transport properties of two-dimensional materials using the AFM. Fu et al. published a paper [2] that showed a change in tunneling resistance with a change in pressure provided by the I-AFM tip. To model the physics the Wentzel-Kramers-Brillouim (WKB) method was used and modified to include the surface deformation caused by the I-AFM tip, as modeled by a hemisphere (see figure 3.1). The experiment was performed on single layer MoS_2. For the author, the experimental motivation was to perform a similar experiment on additional TMD's, in this case WSe_2 and WS_2.

The relationship between force and applied pressure is suggested to have applications in devices such as tunneling Nano-Electro-Mechanical (tNEM) switches. According to these results, a single layer of MoS_2 (monolayer thickness $\sim$.65nm) with a nano-scale mechanical device could be used for such a switch. The advantage to these devices over conventional NEM switches is two fold. First, the MoS_2 monolayer is thin. Second, the mechanical switch used to switch the NEM from on to off can remain in contact with the monolayer. Due to the tunneling relationship shown in figure 3.1, this tNEM switch would not have to completely disconnect with the surface to stop current flow for the off state of the switch. Conventional NEM devices have to disconnect with the material to achieve the same functionality. Disconnection and impact with the surface leads to a more complicated device with lower reliability from effects such as contact material degradation and surface adhesion. With a

tunneling device the resistance decreases by several orders of magnitude with a small application of pressure, allowing the on/off switching capability of the device without the need to disconnect [2].

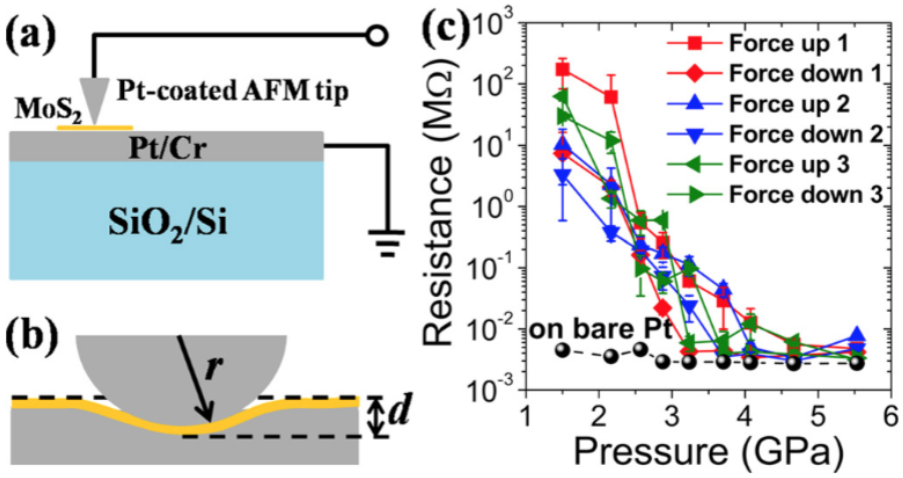

Figure 3.1: Results from Fu et al. The figure shows the experimental setup of the I-AFM for measuring vertical charge transport in MoS_2 (a), hemispherical model used as the tip for tunneling current calculations (b), and the resulting measured resistance vs. applied pressure data. Note the exponential decrease with higher pressure on the sample and the inclusion of data from bare Pt surface for comparison (c) [2].

Looking for correlation between force and vertical resistance in other TEM's could allow additional options for the creation of such devices. Additionally, this experiment looks at a behavior in a vertical transport property in a TEM material. Deformation of monolayers of TEM materials that shows a change in quantum mechanical behavior is insightful into how these materials work at the atomic level.

3.2 Quantum Tunneling and the WKB Approximation

As electronic devices become smaller and smaller, classical physical theory and approximations become less and less reliable for studying such small structures. Quantum effects begin to arise and eventually dominate. For the purpose of explaining the physics in the regime in which the author is performing experimentation, it is necessary to explain the

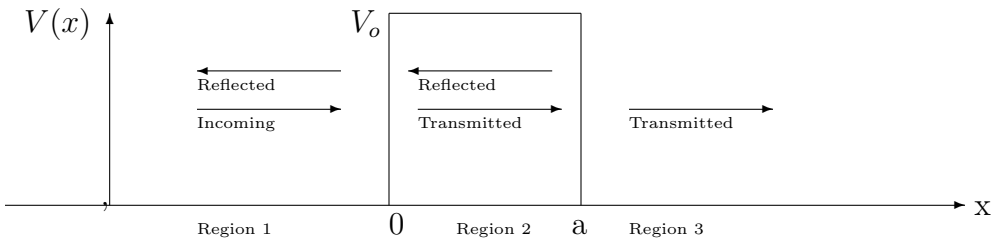

Figure 3.2: 1D Tunneling diagram where the width of the potential barrier is a.

physics behind one model for showing the quantum effect of tunneling in these materials. Quantum tunneling is the chance for, in this case, electrons to "tunnel" through a potential barrier created by the I-AFM tip an the 2D material. This effect can be solved analytically for a square potential barrier. The following solution is for a 1D potential as it is the simplest case of the phenomenon and can be easily expanded to higher dimensionality. Expanding upon this mathematical model will lead to a model usable for this experiment.

To begin, a plane wave representing an singular electron traveling from the I-AFM tip is sent towards the potential barrier. This is modeled by Ae^{-ikx} where k is the wave number, x is the position, and A is the amplitude of the wave. These solutions are applied to the one dimensional time-independent Schrödinger equation in three different regions. Figure 3.2 models the described 1D ideal potential barrier. The wave moves from region 1 to region 3 if it successfully tunnels. The potential barrier is defined to be of width a with a height of V_o and is described by the function $V(x)$. For this ideal example $V(x)$ is a piecewise function.

$$V(x) = \begin{cases} 0 & x < 0 \\ V_o & 0 \leq x \leq a \\ 0 & x > a \end{cases} \tag{3.1}$$

The Schrödinger equation compares the wavefunction of the system with the potential and outputs energy eigenvalues for stationary states of the system (E).

$$\frac{-\hbar}{2m}\frac{\partial^2\Psi(x)}{\partial x^2} + V(x)\Psi(x) = E\Psi(x) \tag{3.2}$$

Using Fig 3.2 as a reference, plane wave solutions are assumed for $\Psi(x)$ for the different interactions the waves have with the potential barrier. At $x = 0$, and $x = a$ we expect an incident and reflected wave with varying intensities as represented by the amplitudes of the waves (A,B,C,D,E). Immediately, due to our assumption that the wave moves from region 1 to region 3, we know A=1 since these are normalized wavefunctions and this initial wave has maximum intensity. Additionally, there is no reflected wave in region 3 (the amplitude of this wave if represented would be 0).

$$\Psi_1(x) = \Psi_{incident} + \Psi_{reflected} = Ae^{i\frac{k_1 x}{\hbar}} + Be^{-i\frac{k_1 x}{\hbar}} \tag{3.3}$$

$$\Psi_2(x) = \Psi_{transmitted} + \Psi_{reflected} = Ce^{i\frac{k_2 x}{\hbar}} + De^{-i\frac{k_2 x}{\hbar}} \tag{3.4}$$

$$\Psi_3(x) = \Psi_{transmitted} = Ee^{i\frac{k_1 x}{\hbar}} \tag{3.5}$$

The boundary conditions that the wave functions and their derivatives must be constant over the boundaries between the regions are applied. In this case the boundaries are at $x = 0$ and $x = a$.

$$\Psi_1(0) = \Psi_2(0), \Psi_2(a) = \Psi_3(a) \tag{3.6}$$

$$\frac{\partial}{\partial x}\Psi_1(0) = \frac{\partial}{\partial x}\Psi_2(0), \frac{\partial}{\partial x}\Psi_2(a) = \frac{\partial}{\partial x}\Psi_3(a) \tag{3.7}$$

The goal is to solve for the wave amplitudes, however, there are not enough equations to solve for all the unknowns, therefore a new quantity is defined called the transmission coefficient (T) ([13], p.218). It is a ratio of amplitudes of the incoming and outgoing wave functions that shows the relative probability for going through the barrier. This ratio can then be used to see the probability that the electron will tunnel. After a significant amount of algebra and simplification the result is:

$$T = \frac{|A|^2}{|E|^2} = \left[1 + \frac{1}{4}\left(\frac{k_1^2 + k_2^2}{k_1 k_2}\right)^2 sinh^2(k_2 a)\right] \tag{3.8}$$

The Schrödinger equation's solution allows for systems to be modeled and thereby explain the physics behind tunneling for such a simple system, however, to successfully describe the tunneling between the TMD and the I-AFM tip an approximation must be made since this barrier is not ideal. One of the ways to handle a non-ideal barrier is the Wentzel-Kramers-Brillouin (WKB) approximation. The method can be used to solve for any potential as it uses classical approximations to the barrier to approximate the tunneling probabilities. It is specifically useful for any system with a slowly varying potential that is effectively constant over a region, which is applicable to the 2D material potential, on the order of the de Broglie wavelength which is defined as:

$$\lambda = \frac{h}{p} = \frac{h}{\sqrt{2m(E - V(x))}} \tag{3.9}$$

The derivation of the WKB method begins with the assumption that the momentum is classical in nature, such that the momentum $p(x) = \sqrt{2m(E - V(x))}$, where $V(x)$ is the potential as in the ideal 1D example and E is the energy of the incoming electron. This approximation is used to find find a solution to equation 3.2 along with the following wavefunction [13].

$$\Psi(x) = A(x)e^{i\frac{S(x)}{\hbar)}} \tag{3.10}$$

Where $S(x)$ is some unknown function representing the phase of the wave and $A(x)$ is the amplitude of the wave. Equation 3.10 is subbed into equation 3.2 and solved leaving the solution:

$$S(x) = \pm \int \sqrt{2m(E - V(x))}\partial x = \pm \int p(x)\partial x \tag{3.11}$$

Using this solution the normalized wavefunction is: (C is an arbitrary constant)

$$\Psi_{\pm}(x) = \frac{C_{\pm}}{\sqrt{p(x)}} e^{\pm \frac{i}{\hbar} \int p(x) \partial x} \tag{3.12}$$

Considering the previous system (see Fig 3.2) and assuming a particle with momentum $p = \sqrt{2mE}$ is headed towards the barrier (m is the mass of the particle), methods similar to the Schödinger solution are employed. The continuity of the wave function in the three regions is a requirement. The major difference is how $\Psi_2(x)$ is treated due to the semiclassical approximation for the barrier. The wavefunctions are replaced with the solution from the WKB approximation (equ 3.12).

$$\Psi_2(x) = \frac{C_{\pm}}{\sqrt{p(x)}} e^{\pm \frac{i}{\hbar} \int p(x) \partial x} + \frac{D_{\pm}}{\sqrt{p(x)}} e^{\pm \frac{i}{\hbar} \int p(x) \partial x} \tag{3.13}$$

Based on boundary conditions the transmission coefficient now becomes:

$$T = \frac{|E|^2}{|A|^2} = e^{-2\gamma} \tag{3.14}$$

$$\gamma = \frac{1}{\hbar} \int_{x_1}^{x_2} \sqrt{2m(V(x) - E)} \partial x \tag{3.15}$$

To fully model the tunneling in the 2D material with an I-AFM tip one more step is necessary. The potential needs to be able to flex under the pressure of the I-AFM tip. Fu et al. uses a specific potential based on the system to apply to the WKB approximation to model this system. This model changes tunneling probability to [2]:

$$T = e^{-2t\sqrt{2m\frac{V_b}{\hbar^2}}} \tag{3.16}$$

Here the potential has been modified as described to model the barrier $V(x) = qV_b$ and subbed into the tunneling solution derived from the WKB approximation. The barrier

thickness defined as t, and m is the carrier effective mass. With this derivation, experiment and theory can be compared.

3.3 Sample Preparation

Based on Berkeley [2] samples were fabricated by a collaboration between Auburn University (Dhar, Kuroda) and the University of Kansas (Zhao) in an attempt to measure tunneling resistance in two-dimensional WSe_2 and WS_2. The sample started as a two inch diameter n-type silicon wafer, which underwent an organic clean, buffered oxide etch, and RCA (Radio Corporation of America) treatment (for details see Appendix A). About 300 nanometers of SiO_2 were then grown on the sample by oxidizing the silicon surface at 1150 °C for four hours flowing O_2 through a tube furnace. The oxide was grown on the silicon surface for coloring, in this case at 300 nm's thick was a blue/purple. The coloring allows optical viewing and characterization of the WSe_2 and WS_2 flakes which would normally be invisible against the non-colored background. Due to the insulating nature of the oxide and the need to pass current through the sample a thin (20-50 $\mathring{A}$) transparent layer of platinum was then sputtered onto 1x1 cm pieces of the oxide. The platinum needed to be thick enough to be conductive, however also thin enough to be transparent. This was achieved by testing 5,7, and 10 second Pt sputters. After this step, IV measurements were performed on the bare platinum coated oxide to ensure conductivity over the entire sample. The ten second sputter met the required qualifications by creating a reliably conductive layer. These pieces were then sent to have flakes deposited onto the platinum layer through exfoliation techniques at the University of Kansas [14]. Once the sample was reacquired, it was mounted onto a standard Park Systems metal sample puck used by the AFM. To mount the sample in place and allow the platinum layer to contact the conductive AFM puck, silver paint was applied to all four corners of the sample and allowed to drape over the edge (See Figure 3.3).

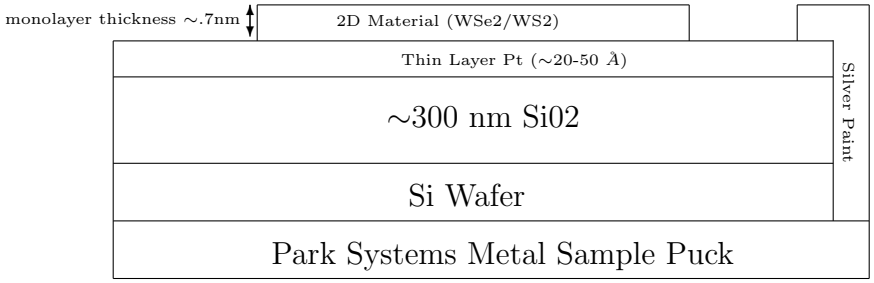

Figure 3.3: I-AFM Sample Diagram (Not to Scale)

3.4 Experimental Procedure

The goal of the experiment is to determine a relationship between force applied to the 2D material and electrical resistance. To accomplish this I-AFM was utilized. The tip used (Rocky Mountain Nanotechnology 25pt300b tip) was made out of solid platinum and mounted on a standard AFM sized ceramic chip. Due to the insulating nature of the ceramic, it is connected to a gold bonding pad with conductive epoxy to allow conductive AFM functionality . The tip has a tip diameter guaranteed < 10 nm, however packaging and SEM of the tip included guarantees <8 nm and a spring constant of 18.0 N/m $\pm$ 7.2 (40%) [7]. The Park Systems XE7 microscope is fitted with an external module to process the current data from the tip. The head is also fitted with an attachment to be able to send the current from the tip to an external module (see Appendix B Section B.4). The functionality of applying a bias from the sample stage is retained.

To verify the systems functionality, initial scans were performed on a test sample of Highly Ordered Pyrolytic Graphite (HOPG). Initial scans showed promising performance. Changing the bias on the sample stage increased current measurements in the HOPG. Once verified, the sample (see Figures 3.3 and 3.4) was mounted onto the AFM stage. The AFM stage is magnetic and therefore sticks to the sample puck to reduce movement of the sample during scans.

Figure 3.4 shows optical images of the WSe_2 and WS_2 flakes that were sent as reference images. The layer thicknesses were determined optically based on contrast values. Using the AFM's optical microscope, they were located amongst many other flakes deposited on the

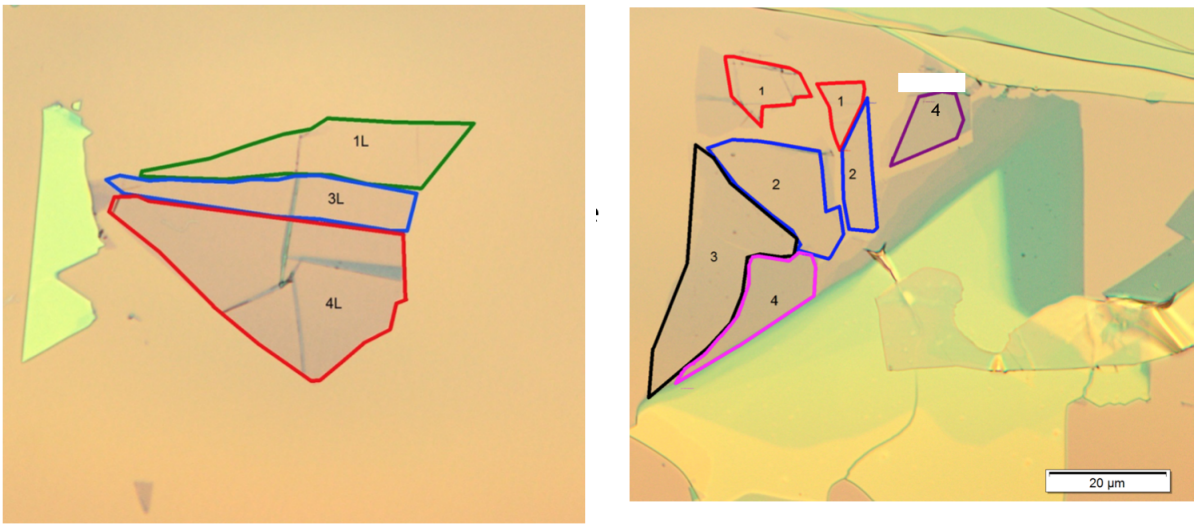

Figure 3.4: Optical Images of Left:WS_2 Flake Right:WSe_2 Flake with layer thicknesses labeled [14]

surface. The green regions, without labeled layer thickness, are many layers thick (50 to 100 layers based on profiles from the AFM). The orange is the bare Pt surface.

10x10 μm and 5x5 μm areas were initially scanned at 811 nN (default for the 25pt300b tip) force constant on the tip for a topographical image. Each of these images were taken to ensure uniform layer thickness over the entire area. After this step, for the majority of measurements, the I-AFM was put into IV scan mode allowing the scan of the AFM tip to stop and to take localized IV curves. Voltage range was limited to $\pm$ 20 mV and current was limited to 0.1 μA for these measurements. The set point was then changed, thereby changing the force applied to the I-AFM tip, and the IV measurement was repeated. Various experiments tried different measurements, which I will outline below. Later on an experiment was performed where force was held at a constant over a 5x5 μm scan with biases of 0, 10mV, and 20mV applied to the back of the sample through the stage. Most of the experiments were performed on the WSe_2 sample.

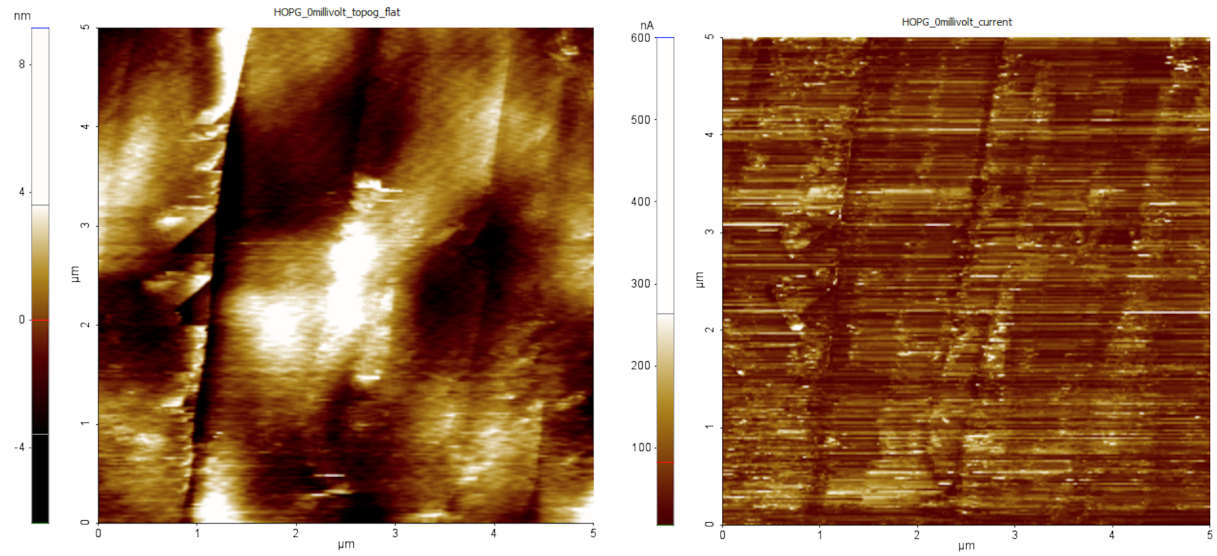

Figure 3.5: Left: 5x5 μm scan HOPG 5mV sample bias topography Right: 5x5 μm scan HOPG 5mV sample bias current

3.5 Results and Discussion

As mentioned earlier, to verify tip functionality a standard sample, in this case a piece of HOPG, was used to verify that the I-AFM measured appropriate topography along with conducting current. One of the resulting scans is shown in figure 3.5. Due to the high conductivity of the HOPG a low bias of 5 mV was applied to the back of the sample. Before the scan the top layers of the HOPG were exfoliated with scotch tape. These scans allowed the author to verify tip functionality while also allowing practice with the the setup of I-AFM.

As mentioned previously, the platinum layer was verified to be conductive though IV measurement. Once the TMD's were applied to the sample it was still necessary to take initial I-AFM scans to verify the continued conductivity of the sample as well as verify that I-AFM could be performed on the flakes. Figures 3.6 and 3.7 show the resulting scans. The 25pt300b tip allowed single to four layer flakes to be imaged and visible in the topographical image. The corresponding current profile also showed the conductivity of the platinum layer under the flakes. Bias was also applied to the samples, although current was measured in

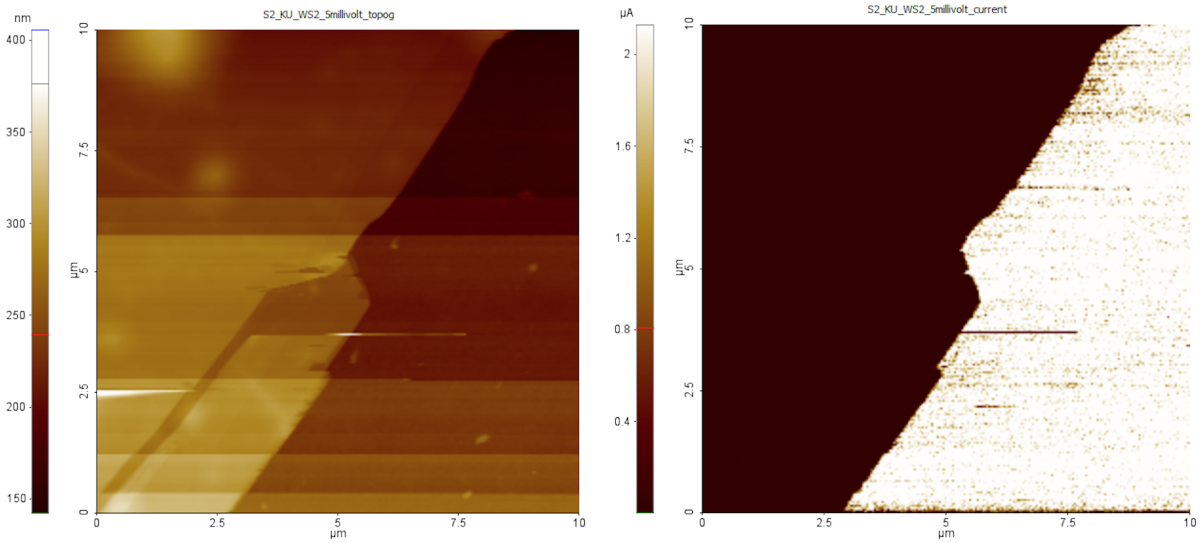

Figure 3.6: Left: WS_2 Flake 10x10 μm Scan Right: WS_2 10x10 μm Current Scan 5mV Sample Bias

the scans without a sample bias. This allowed the I-AFM to show the differences in the current profiles from the bare platinum and the WSe_2 flakes. The platinum layer is making an electrical short, so at this point it was necessary to keep the tip on the flakes to avoid possible damage to the AFM and tip during prolonged use.

The next step involved positioning the I-AFM at several localized points determined by the current scan. At these points the I-AFM tip was held still for localized IV measurements. Based on [2] multiple IV curves needed to be taken at various forces to measure the tunneling current due to the deformation of the flake. This tunneling current would be detected by a change in resistance as the force changed. To accomplish this the I-AFM tip was positioned and held still. An IV sweep from -20 mV to 20 mV was taken with a limit on the current of 0.1 μA. The force was then changed by variation of the force set point of the I-AFM before the next IV was taken. Each IV was taken as two IV's, one increasing bias, then reversing. The first experiment was done on the three layer WSe_2 flake and the force was varied from 800 nN to roughly 0 nN. Resistances from the IV's were taken from fitted slopes (the resistance in this case was the inverse of the slope) over a -5mV to 5mV range. Results showed a possibly

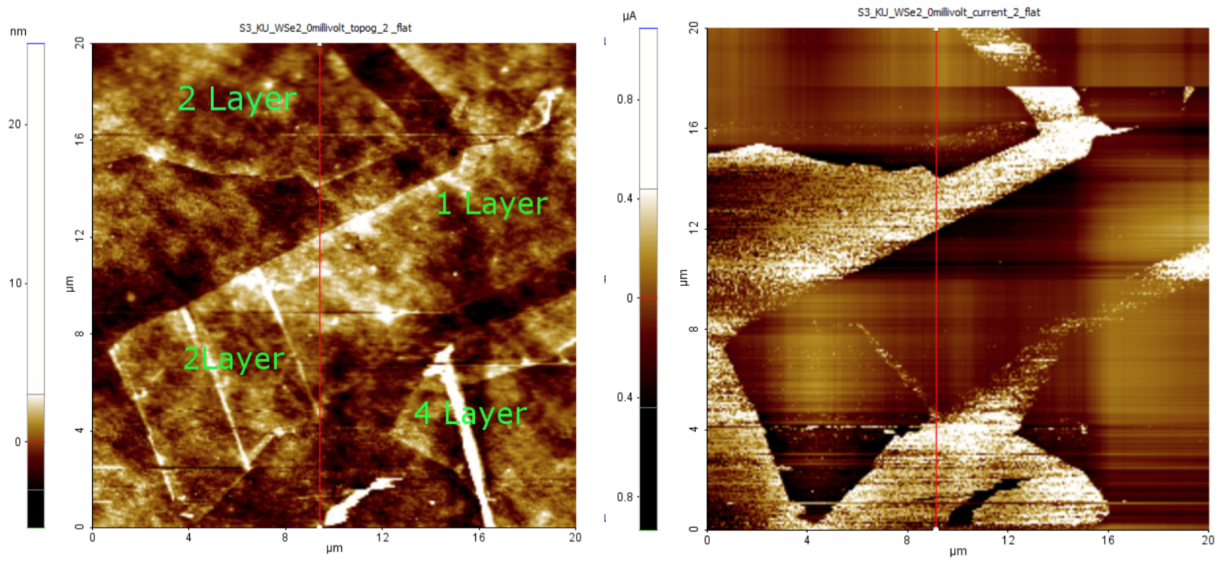

Figure 3.7: Left: WSe_2 Flake Topgraphy 20x20 μm scan Right: WSe_2 current map 0 mV 20x20 μm scan

promising trend due to the exponential decay of the resistance with greater force and the range of resistances measured (see figure 3.8). Based on these results the author aimed to show this trend on other flake layers, however the range of forces was limited to 500 nN since the trend of the resistance data stopped at 350 nN in this set of data. Concerns of damaging the flake also encouraged the limitation of the force applied by the tip. This concern was later explored by looking for a hysteresis trend in the resistances measured and discounted.

On repeating the experiment on with the above mentioned modifications on the same three layer flake, as well as other layers, problems with reproducibility began to show (see figure 3.11). Variation in IV curves and resistances, even in IV's taken on the same spot in succession, showed differences (see figure 3.9). As mentioned, damage to the flake was suspected. Repeated scans varying the force and bias were conducted to see if a hysteresis behavior existed. No hysteresis trend was found. Eventually, to see how much variation existed, IV curves were taken at the default force set by the I-AFM on each of the layer thicknesses (see figure 3.10). The figure shows the variation to one standard deviation. Each point represents the mean of multiple IV scans taken at a singular spot, which varied between

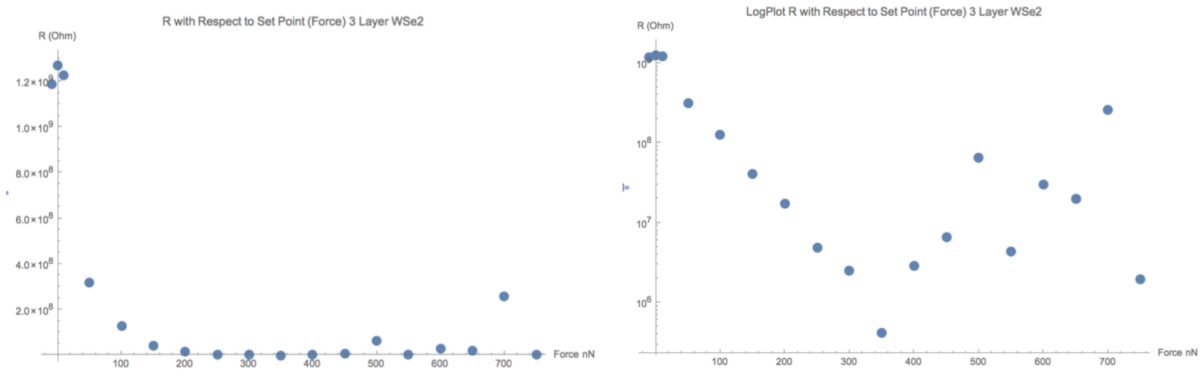

Figure 3.8: Resistance vs Force Data from Three Layer WSe_2

2-4 IV curves (see the chart in figure 3.10) based on how many of the 4 were ohmic in the ± 5 mV range. These results showed that reproducibility of the initial experiment was, at this point, unachievable.

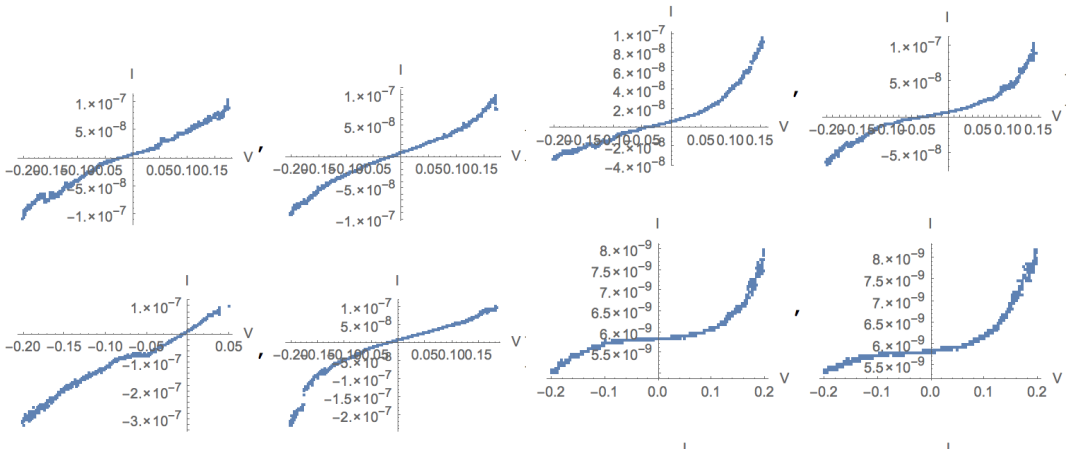

Figure 3.9: Left: IV Curves 1 Layer WSe_2 -20 to 20 mV Right: IV Curves 4 Layer WSe_2 -20 to 20 mV (I has units of Amps, V has units of Volts)

The next step was to look at the statistical variation of many more IV curves by utilizing the I-AFM functionality. On each flake 5x5 μm scans were taken at 0,10, and 20 mV sample bias with no current limit set on the I-AFM tip due to the lack of instrumental control in this mode. The force was also varied. For each scan a mean current was determined. Upon looking at the results, each scan showed a complete spectrum of current ranging from nano

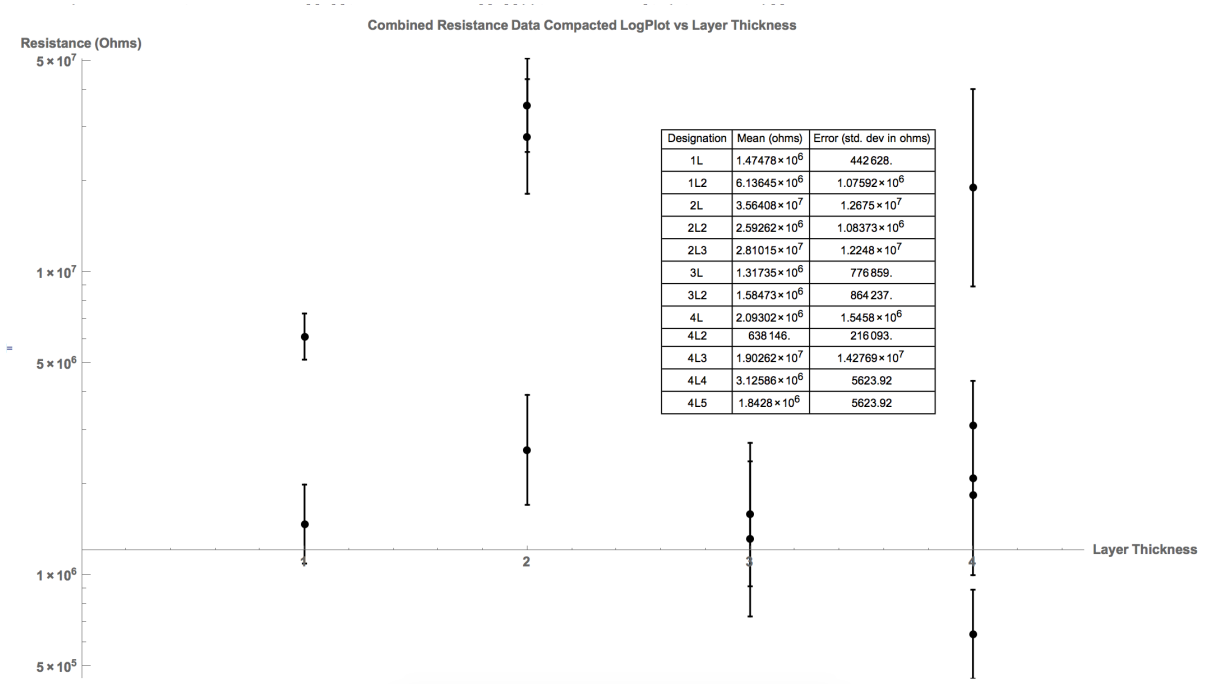

Figure 3.10: Variance to one Standard Deviation of Resistance at 811 nN force

amps to two microamps where the I-AFM tip maxed out, which was only hit due to the lack of a current limit setting. Attempts were made to limit the current in post image processing, similar to the method employed in the IV curve method described previously. With these large currents removed in image processing, it was noticed that all scans showed very similar behavior (mean current .48 μA), independent of force or bias applied to the sample.

At this point it is necessary explain and reinforce the underlying principle behind scientific endeavors and progress. The underlying principle of this method is the idea of reproducibility. Science does not seek truth or causation in specific isolated examples. Without reproducibly of data, no conclusion can be drawn. Many attempts were made to find reproducible data that matched with the original motivation as provided by other members of the scientific community. Further research with more refined techniques may be able to continue such work to discover more of the underlying principles, however, the author was unable to produce reproducible, consistent, or correlated data from this experiment and therefore must discount any useful progress or analysis from this endeavor.

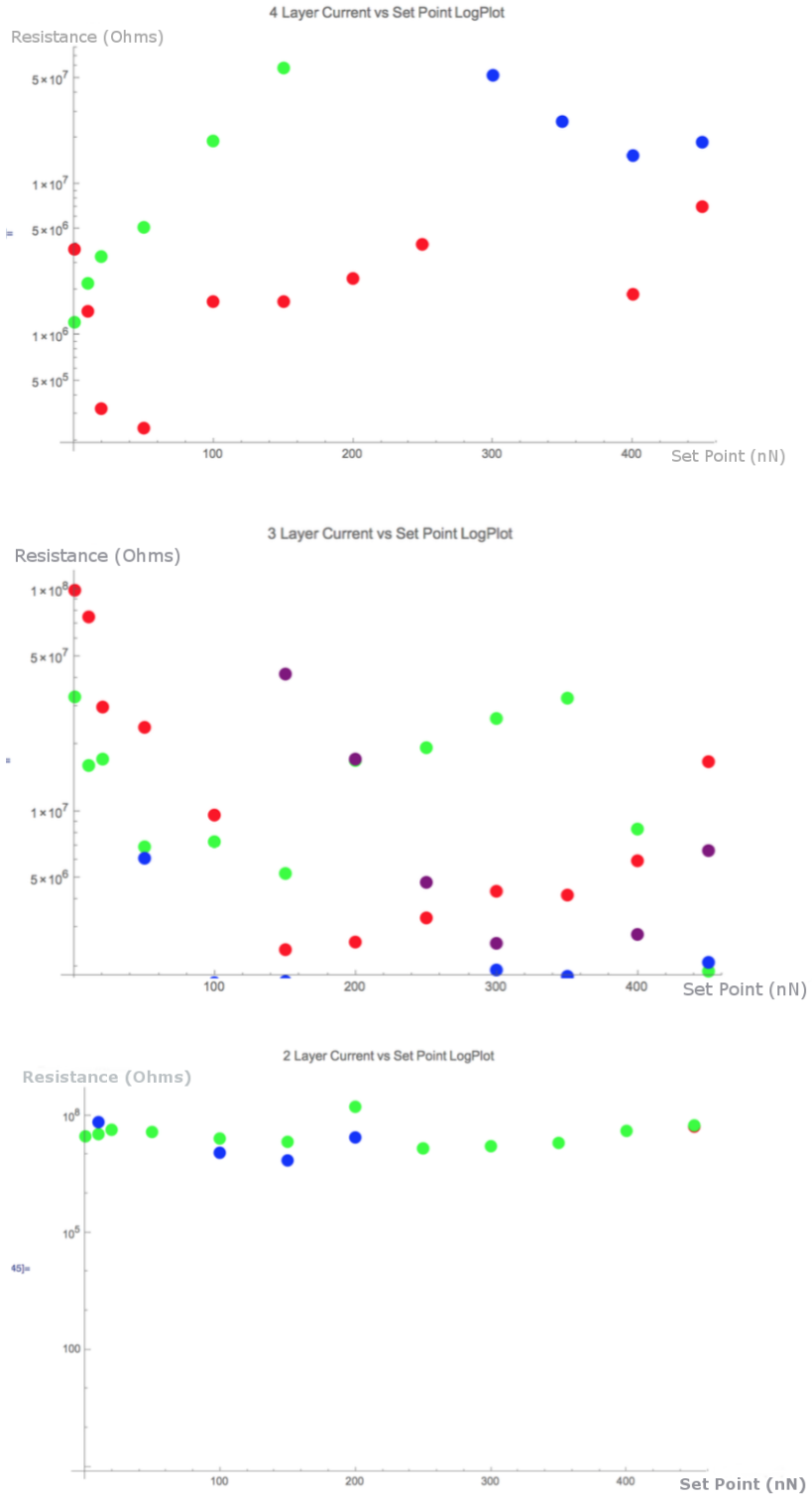

Figure 3.11: Top: Resistance vs Force 4 Layer WSe_2 Middle: Resistance vs Force 3 Layer WSe_2 (Purple Data points are the same as fig. 3.8) Bottom: Resistance vs Force 2 Layer WSe_2 (Different colors represent different runs on different spots on the WSe_2 flake at that layer thickness)

Chapter 4

Thickness Measurement of Ultra-Thin Boro-Silicate Glass Films on SiC

4.1 Motivation for Experiment

Surface roughness measurements as well as profile measurements are used to show connections between the annealing techniques, physical properties of the surfaces, and electrical properties gained by performing such processes. Verification of structural details in the surface and interface of the materials used to make devices can give reasoning as to why a device performs in an unexpected way, or verify improvements in the conditions of the device at various stages of fabrication. In this chapter an example of such characterization, using NC-AFM, is presented on Boro-Silicate Glass (BSG) films grown on SiC.

Although the structure of a MOSFET is generally standard, the quality of the interface between the oxide and the semiconductor can have drastic effects on the functionality of the device. In 4H-SiC MOSFETs channel mobility is very low, which is unfavorable for electronic devices, especially high power devices. One way to improve mobility of electrons in the channel is to experiment with the annealing process used to form the oxide. It is suspected a major cause of this low channel mobility is the abundance of traps near the interface between the oxide and the SiC [6]. These traps are caused by deformities in the interface, which effect device functionality. Annealing, if done properly, allows some of these traps to be healed or oxide to be grown with less traps. The industry standard is NO annealing, and it has been shown to be effective in SiC [8]. Experiments have also shown the growth of Phospho-Silicate Glass (PSG) to improve channel mobility [10]. For this experiment another method is being examined. Instead of using a NO or N_2O source for the anneal, a boron source is used. The process creates BSG as the oxide for the device.

The author used the AFM to classify the results of the annealing process to characterize the growth process of this oxide.

While NO annealing does increase channel mobility in SiC MOSFETs, improvements can be made with a Boron source [6] or a phosphorus source [10]. For the samples seen by the author, further improvements can be seen with the use of a Boron Oxide Source (B_2O_3) in certain measurements. Passivation and device functionality is evaluated by measuring current between source and drain with a fixed potential difference while varying the gate voltage (V_g), which is the voltage needed to be applied to the gate of a MOSFET. The mobility of the device can be determined from this quantity [6]. Generally a higher mobility is preferable as it leads to more current for faster switching speed. The BSG shows higher mobility in the devices tested than devices passivated with NO or not at all.

4.2 BSG Oxide Instability

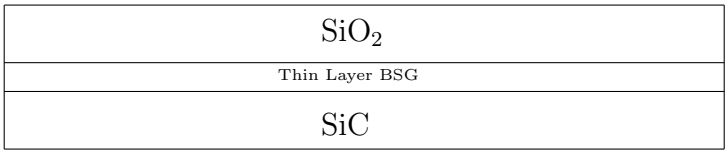

Figure 4.1: Proposed layering of oxide for BSG device (relative layer thickness not represented)

Despite better electrical characteristics, the problem with BSG is instability in the oxide with applied bias. To further improve the process and possibly remove some of the instability issues another experiment was proposed. SiO_2, the oxide from which the BSG is formed in the previous process, has high stability. The idea is to still use the SiO_2, however, to also take advantage of the the BSG SiC interface to lower trap density. To do this, a thin layer of BSG must be grown on the SiC, and afterwards SiO_2 can be grown on the sample, effectively sandwiching the thin BSG layer between the SiC and the SiO_2 (see figure 4.1). A balance

between layer thickness and boron concentration needs to be reached for this method to be tested.

The samples were created by first growing a layer of SiO_2 on the surface of the SiC. This was done by oxidizing the SiC surface by flowing O_2 through a tube furnace for 2 hours at a given annealing temperature. Annealing temperatures are shown in table 4.1. The sample is then moved to another furnace and exposed to the B_2O_3 source at lower temperatures. The boron deposits into the SiO_2 forming BSG on the SiC surface, replacing the SiO_2 if given enough time. To create the step height for the AFM to measure, portions of the sample were screened from this process, allowing bare SiC to be exposed next to the BSG. This is the boundary the AFM scanned over and the results are shown in figure 4.1 and table 4.1.

The author took 10x10 μm AFM topographical images at the boundary of the oxide and the SiC on four samples (see figure 4.3) As seen in table 4.1 the thickness of the oxide decreased with layer thickness while boron concentration remained constant (8-9%). The small peaks on the surface, seen as white dots in the images in figure 4.3, appear on the SiO_2, BSG, and SiC surface and are between 40-50 nm in height as measured by the AFM. These are real features, although their actual height maybe smaller due to the AFM not being able to track the topography change quick enough. The fact that they appear at all stages of the growth of this oxide indicate that either these are defects from the original SiC surface, or grow during the the initial growth of the SiO_2 on the SiC.

Sample	Oxidation Time	Oxidation Temperature	Boron pre-deposition	Boron Drive in Time	Oxide Thickness (nm)	Boron Concentration
O1	2hrs	950 °C	30 min	1hr	2.77	8.1%
O2	2hrs	1000 °C	30 min	1hr	5.77	8.2%
O3	2hrs	1100 °C	30 min	1hr	6.95	9.6%
O4	2hrs	1150 °C	30 min	1hr	11.74	9.2%

Table 4.1: Table of BSG Oxidation Techniques as it relates to oxide thickness and boron concentration

4.3 Results and Conclusion

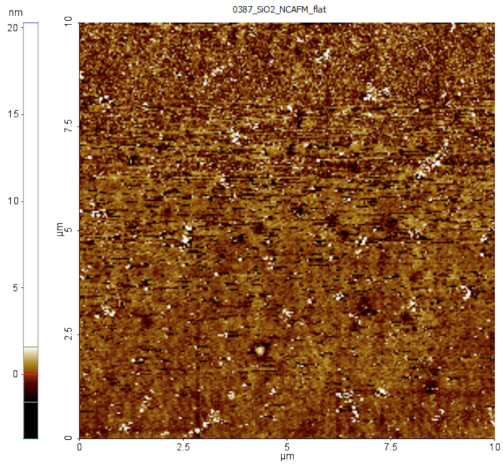

Figure 4.2: Scan on interface after etch of oxide

As stated, the process of creating the BSG involves growing a layer of $Si0_2$ on the sample. With the introduction of boron, the oxide and SiC combine with the boron to generate a layer of BSG on the surface of the SiC. Based on this process the interface should be fairly smooth and therefore less likely to have defects at the interface, hence less traps. After electrical measurements were made, the oxide was removed from the devices with an etch. This allowed the author to use the AFM to look at the roughness of the interface between the oxide and the SiC more closely. The surface which was the interface between the SiC and the BSG is very smooth as shown in fig 4.2 (RMS roughness .8nm).

From Table 4.1 we can see the results of the characterization. Boron concentration remain roughly the same despite oxide thickness, showing that based on the annealing temperature thin layers of BSG can be grown while maintaining the effectiveness of the oxide. Additionally, the AFM results show the changes in layer thickness when the Boron is not present. This change in layer thickness will help in the process of growing oxide for these new devices.

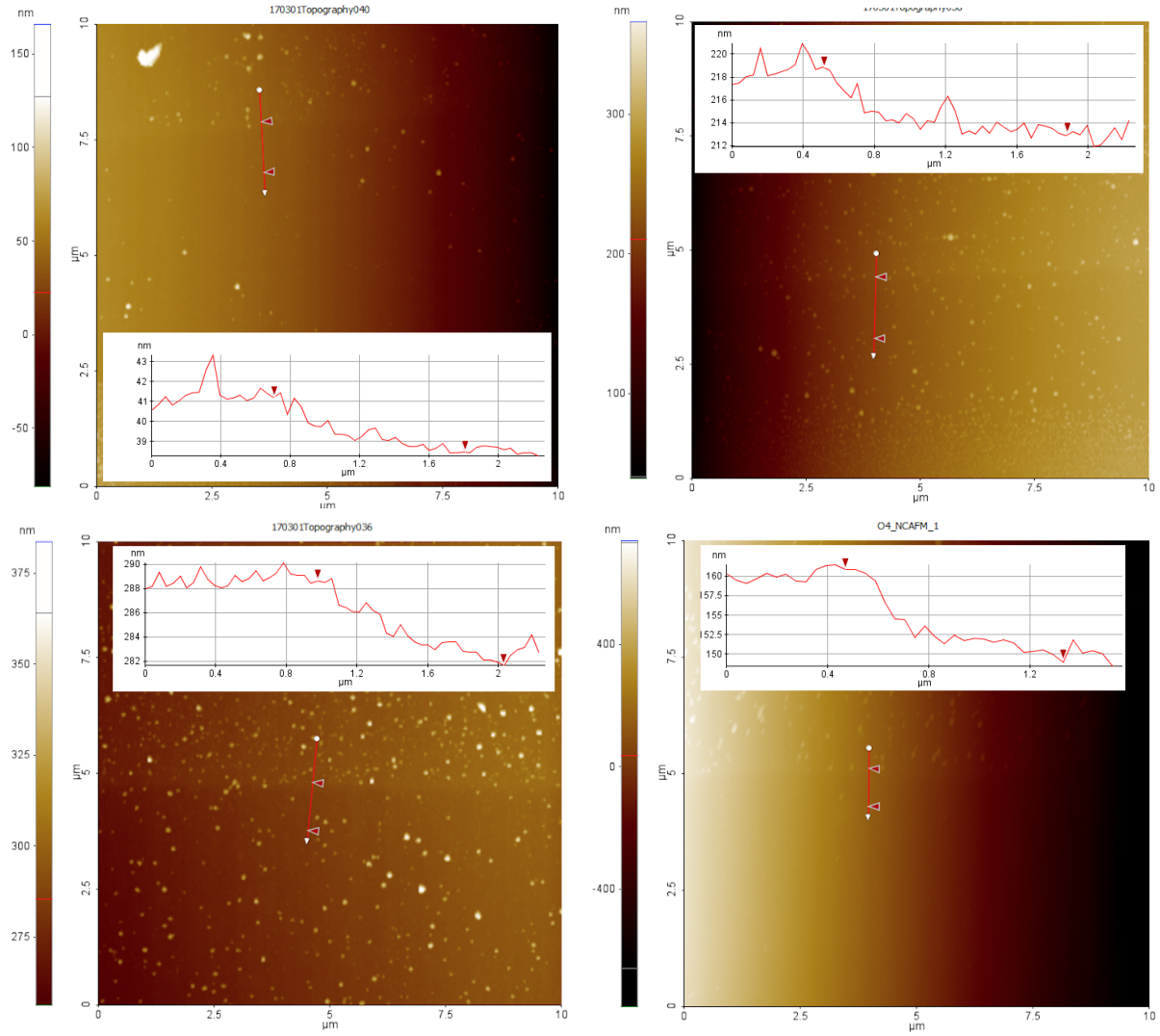

Figure 4.3: Images showing different topographies from which step heights were taken on BSG samples, profiles overlayed. All images 10x10 μm NC-AFM images. Top Left: 900 °C anneal (O1) Top Right: 1000 °C anneal (O2) Bottom Left: 1100 °C anneal (O3) Bottom Right: 1150 °C anneal (O4)

Chapter 5

Conclusions

The main achievement the author has reached is a deep and masterful understanding of the capabilities and uses of the AFM and its subsidiary specialities, specifically with the XE7 AFM. The experimental data from the MoS_2 tunneling current measurements by Fu et al. are not reproducible on WSe_2 at this point. Measurements taken on the BSG samples have helped in the characterization of the passivation of defects that limit channel mobility in SiC MOSFET devices. The experiment has shown that thin BSG films can be grown while maintaining oxide functionality as measured by boron concentration in the layer. BSG MOSFET devices show promising mobility characteristics, better than the current prominent process of NO annealing, and with these thin layers, maybe some of the instability issues will be fixed. These topics are at the brink of understanding in this particular area of condensed matter physics.

The AFM is one characterization method, and many different measurements and characterizations are necessary to understand the basic principles of the nature of these devices and materials. During the creation of this thesis the author has been able to help with that process by understanding and providing this characterization method.

Future work can be conducted on the WSe_2 and the WS_2. Based on the data collected in this experiment, the author would suggest future work that looks at the interface between the Pt and the TMD before new samples are created. The measurement of tunneling current in these materials has turned out to be difficult and variable, however, relationships between pressure and current similar to those shown in MoS_2 may still exist. Understanding how the layer connects with the Pt layer may explain why the measurements vary so much. Immediate future work can include image processing on the 5x5 μm I-AFM scans taken on

the different layers of WSe_2. As to the BSG experiment, the author has already participated in experiments that vary the annealing technique once again to by creating Phosphosilicate Glass (PSG) instead of BSG on the surface for similar electronic applications. MOSFET devices have been created with BSG and tested. This work already continues and further characterization with the AFM to help this process can always be done.

Bibliography

[1] EFM Electrostatic Force Microscopy for XE Series SPM Santa Clara, CA: Park Systems Inc, 2004. Print.

[2] Fu, Deyi, Jian Zhou, Sefaattin Tongay, Kai Liu, Wen Fan, Tsu-Jae King Liu, and Junqiao Wu. "Mechanically Modulated Tunneling Resistance in Monolayer MoS2." Applied Physics Letters 103.18 (2013): 183105. Web.

[3] Giessibl, Franz J. "Advances in Atomic Force Microscopy." Reviews of Modern Physics 75 (2003): 949-83. Print.

[4] Lin, Zhong, McCreary, Amber, Briggs, Natalie et. all. "2D materials advances: from large scale synthesis and controlled heterostructures to improved characterization techniques, defects and applications." 2D Materials 10.1088 (2016):042001. Web.

[5] Novoselov, K. S., Geim, A. K., Morozov, S. V., Jiang, D., Zhang, Y., Dubonos, S.V, Grigorieva, I. V. and Firsov, A. A. (2004) Electric Field Effect in Atomically Thin Carbon Films, Science 306(5696): 666-669.

[6] Okamoto, Dai, Mitsuru Sometani, Shinsuke Harada, Ryoji Kosugi, Yoshiyuki Yonezawa, and Hiroshi Yano. "Improved Channel Mobility in 4H-SiC MOSFETs by Boron Passivation." IEEE Electron Device Letters 35.12 (2014): 1176-178. Web.

[7] Rocky Mountain Nanotechnology, LLC. N.p., 2016. Web. 24 May 2017. <http://rmnano.com/>.

[8] Rozen, John, Ayayi C. Ahyi, Xingguang Zhu, John R. Williams, and Leonard C. Feldman. "Scaling Between Channel Mobility and Interface State Density in SiC MOSFETs." IEEE Transactions on Electron Devices 58.11 (2011): 3808-811. Print.

[9] SCM Scanning Capacitance Microscopy for XE Series SPM Operating Manual. Santa Clara, CA: Park Systems Inc, 2004. Print.

[10] Sharma, Y. K., Ahyi, A. C., Isaacs-Smith, T., Modic, A., Park, M., Xu, Y., ... Williams, J. R. (2013). High-mobility stable 4H-SiC MOSFETs using a thin PSG interfacial passivation layer. IEEE Electron Device Letters, 34(2), 175-177. [6407723]. DOI: 10.1109/LED.2012.2232900

[11] West, Paul, and Natalia Starostina. A Guide to AFM Image Artifacts. Santa Clara, CA: Pacific Nanotechnology, n.d. PPT.

[12] XE7 High Accuracy Small Sample SPM User's Manual. 2.0.0 ed. Santa Clara, CA: Park Systems Inc, 2013. Print.

[13] Zettili, Nouredine. Quantum Mechanics: Concepts and Applications. 1st ed. West Sussex: John Wiley and Sons, 2001. Print.

[14] Images and flake deposition courtesy of Dr. Hui Zhao University of Kansas.

Appendices

Appendix A

Silicon Wafer Cleaning

A.0.1 Organic Clean

1. Acetone 5 minutes
2. Tricloral Ethlyene (TCE) 5 minutes
3. Acetone 5 minutes
4. Methanol 1^{st} dip 5 minutes
5. Methanol 2^{nd} dip 5 minutes
6. De-Ionized water (DI H_2O) 5 minutes

A.0.2 Buffered Oxide Etch

1. Boron Oxide Etch (BOE) 5 minutes
2. DI H_2O water 5 minutes

A.0.3 RCA Cleaning

1. Equal parts Sulfuric Acid H_2SO_4 and Peroxide H_2O_2 15 minutes
2. DI H_2O water 30 seconds
3. BOE 1 minute
4. DI H_20 water 30 seconds
5. 10 parts H_2O, 3 parts peroxide H_2O_2, 3 parts Ammonium oxide NH_4O_2 on hot plate 15 minutes
6. Repeat steps 2-4
7. 10 parts H_2O, 3 parts peroxide H_2O_2, 3 parts Hydrochloric Acid HCL also on hot plate 15 minutes
8. Repeat steps 2-4

Appendix B

AFM Users Manual

The following is a step by step guide to running the XE7 AFM with commentary by the author. It is meant to aid in the use of the AFM in all modes available at the current date at Auburn University as well as give clarity to methods employed by the author in creation of this thesis. **For each setup, the AFM will start in C-AFM mode and then modified for other uses.** If there are any questions about these instructions, please reference the users manuals provided by Park Systems.

B.1 Basics

Before every use of the AFM make sure the following conditions are met: The AFM is on (there is a green power button on the main electronics box), the XEP software is open (note this must be opened after the AFM is turned on otherwise it will show an initialization error. If this happens make sure the AFM is on, then close and reopen the XEP software), and the FlyPoint Capture software is open (this is the feed to the optical microscope of the AFM).

B.2 C-AFM and Taking a Scan

C-AFM is the most basic and straightforward setup for the AFM. In this section I will describe basic scanning and functionality for the AFM to be used with modification for the following sections.

Before taking a scan always check the height at which the tip is at via the Z Stage window (see figure B.3), that the PSPD is aligned, and that the sample is in roughly the correct position.

1. To change a C-AFM tip proceed through all steps in the AFM Head Removal section. Then refer to the NC-AFM section steps 2-7 but install the C-AFM tip since the process is the same, however, no frequency sweep window will pop up in step 6. Finally proceed through all steps in the Laser Alignment section.

2. The first step is to focus the optical microscope onto the sample. To do this however, the Z Stage needs to be lowered closer to the sample, otherwise the optical microscope will run into the Z stage before it is focused on the sample.

3. The Z Stage window has a graphic (see figure B.3) of what looks like an AFM tip. This is a usable graphical object. The black line at the center indicates the boundary between moving the tip up and down. Clicking below the line will move the stage

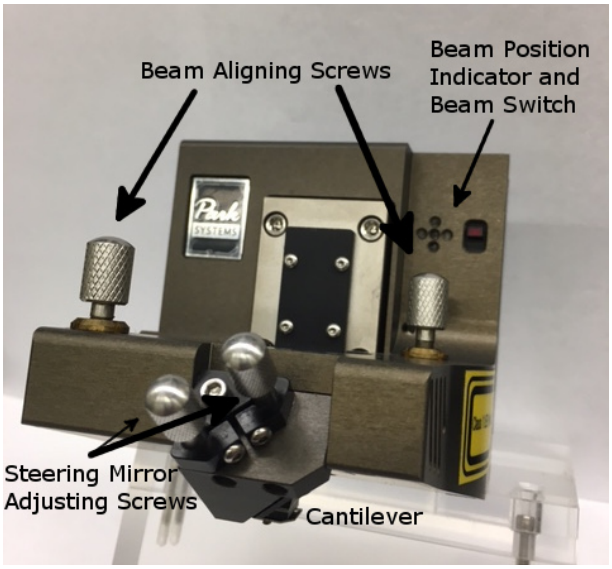

Figure B.1: Labeled XE7 AFM Head

down, the farther from that line the faster it moves. Note: if the PSPD is not aligned properly the stage will move slowly or show an error message and refuse to move. This is a safety feature that looks for sudden changes in the intensity of the laser, keeping the AFM tip from crashing into large topography on a sample.

4. Click below the Black line while watching the AFM tip approaching your sample by actually looking at the stage as it approaches the sample. The AFM tip needs to be within roughly 1000 μm of your sample surface for the focus of the optical microscope to be in range. Once the stage is close to the sample, turn the optical microscopes focusing knob to focus on the sample. If the sample doesn't come into focus without crashing into the stage, lower the stage further.

5. Using dials on the sample stage move the sample to the desired scan position. More precise scans can be achieved by focusing on the AFM tip briefly and using a non-permanent dry erase marker on the computer screen to indicate where the tip is and refocusing on the sample. Note: different AFM tips have the actual projection at different places, refer to details from the manufacturer to determine this. Usually there is a SEM image of the tip included in these details.

6. Verify the PSPD is aligned. Scan parameters such as size and rate can be changed as well.

7. Close and latch the front door to the AFM sound proofing box.

8. Hit the approach button located at in the Z Stage window (see figure B.3). The AFM will automatically do the final approach to the sample surface. This can be canceled at any time by re-clicking the approach button, which will now say Cancel. If the stage starts bouncing (moving in small steps), this can be determined optically or by looking

at the Z scanner graphic next to the PSPD (it shouldn't be jumping all over the place) simply cancel the approach and hit approach again.

9. Now that the Tip has successfully reached the sample surface, a blue and yellow line will appear in the Trace window. For C-AFM there will only be once trace window with topography. The Blue line represents the left to right movement and the Yellow line represents the right to left. To have a successful scan both of these lines should match.

10. First hit the Auto button next to the slope control in the Scan Control window (see figure B.2). This will automatically correct for any slope that sample might have. If it is having trouble, there is a manual control for the slope to the right of this button.

11. Now hit the Auto button, or manually control the scaling of the image in the topography trace window. This will adjust the scaling so the topographical features of the sample are visible.

12. As stated previously the Yellow and Blue lines in the trace window need to be similar, indicating that the AFM is measuring the same topography in both direction of it's scanning motion. In C-AFM the main tool to help with this is the Gain, although the author has noticed that changing the direction of the scan to vertical (by clicking the Y button at the top of the scan control window) tends to give the tip more stability. The Gain is controlled by the Z Servo Gain control also located in the Scan Control window (see figure B.2). **The Z Servo Gain must stay below or equal to 2.000 for any scan in any setup of the AFM.** Also notice that the number input into any scan parameter for the AFM will not take effect until you hit enter on the keyboard.

13. Now click the Image Start button or the Scan Here button to initiate the scan. This button will turn into a button that states Cancel and can be used to cancel the image at any point.

14. Once the scan finishes it will be stored in a buffer. Right clicking on these images will give an option to send the image to XEI, the image processing software provided by Park Systems where it can be analyzed and saved in an appropriate location. Note: after the scan finishes the AFM rescales the color palette for the image and will seem to destroy the image. To see more of what was seen while taking the scan, either slide the color controls on the sides of the images or flatten the image in XEI (refer to the XEI section for details).

15. The AFM has now performed a successful scan. To move to another area, either use the Offset buttons for around 10 μm of freedom or press the Lift Z button (see figure B.3) and repeat the approach and scanning proceedure.

B.3 NC-AFM

To change the AFM from C-AFM to NC-AFM requires a change of tip, changes in the XEI software, and a laser realignment.

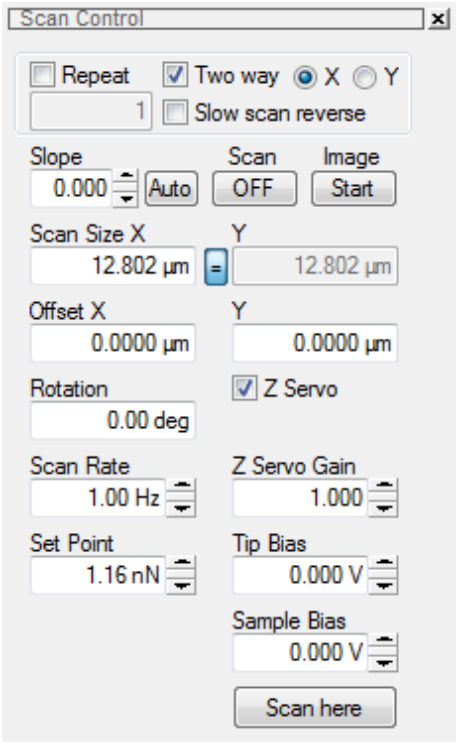

Figure B.2: C-AFM Scan Control Window

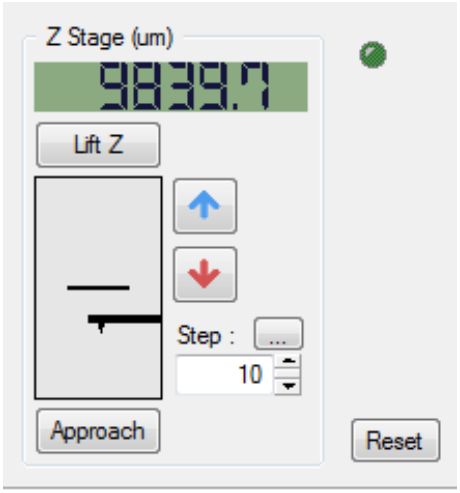

Figure B.3: Z Stage Interface

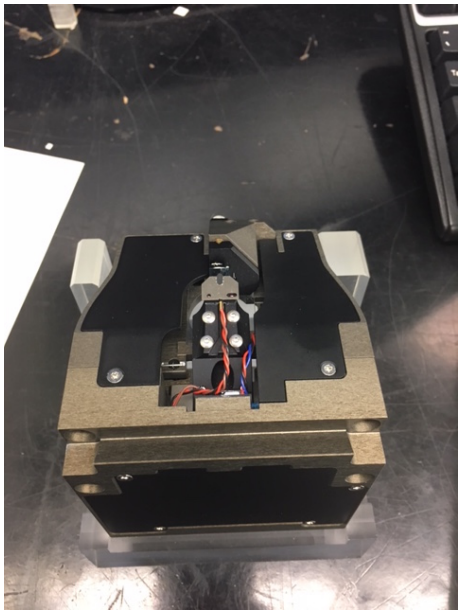

Figure B.4: C-AFM tip installed

1. Proceed with all steps in the AFM Head Removal section.

2. Remove the C-AFM tip from the magnetic holder with a pair of tweezers. Place the tip into the box with the AFM tip down (the small black portion). Bottom row is designated Used tips, top is Broken tips, and bottom is New tips. Replace the C-AFM tip with a NC-AFM tip. The metal base on which the tip is attached will stick to the head of the microscope. Align the two holes in the metal base to the two projections on the head of the microscope (see figure B.5).

3. Carefully replace the AFM head by sliding it from right to left along the rails until it stops. Move the plastic tabs backward to their original position and reattach the power cable to the side of the AFM head.

4. Click on the drop down menu next to the icon used to turn the head off, set the system to NC-AFM. The software will prompt you to make sure you wish to change the mode of the head (see figure B.6).

5. Now go to Setup, then Part Config. Open the dropdown menu next to Cantilever. This will show all AFM tip types known to the XE7 Software. Look at the box from which the NC-AFM tip came from. On the label will be an identifier called Item. This is the type of tip in the box. Find this in the dropdown menu and select it. Note: the item names will not match perfectly since they will sometimes have identifying letters in front or at the end of the name of the tip such as PPP, 5M, 10M, etc.

6. Once you are sure you have told the system what mode it should be in and what tip is installed, turn the head back on. Upon doing this the XEP software will update its interface and a Frequency Sweep window will pop up. Hit Done on the Frequency

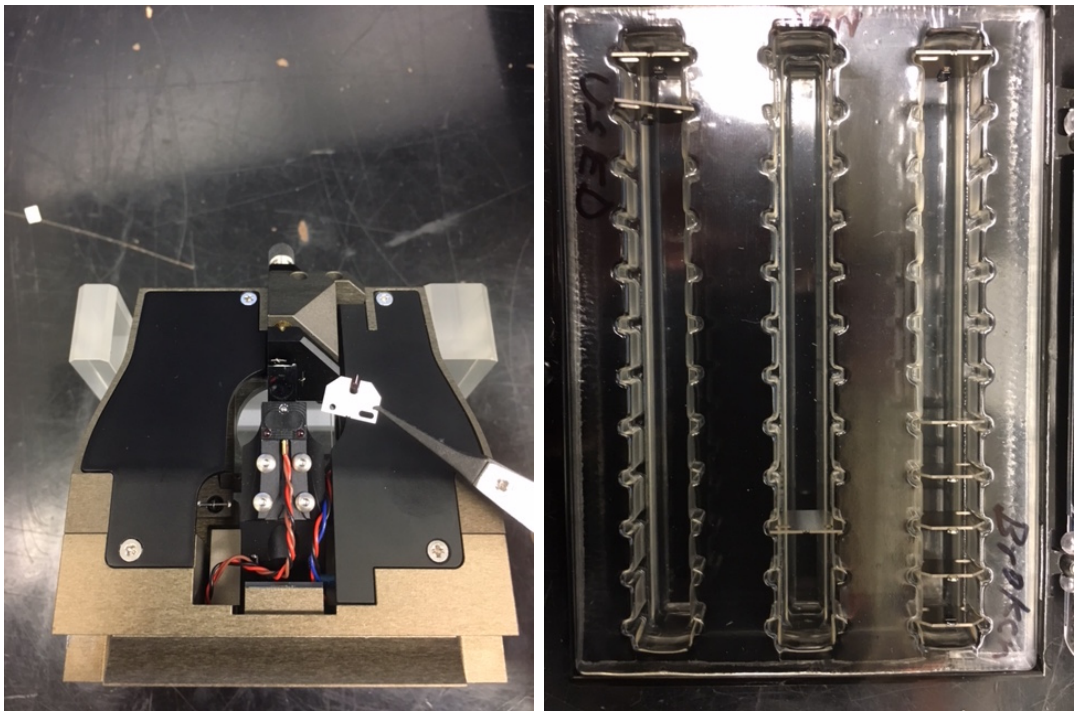

Figure B.5: Removal of AFM Tip from Head Assembly

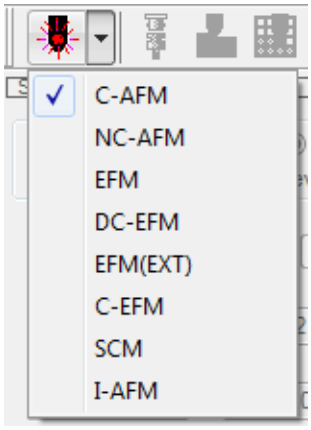

Figure B.6: Headmode Switching drop down menu

Sweep window to close it for the moment. The laser is not aligned at this point (or on for that matter if you manually turned it off) so it will not show a nice curve, required for NC-AFM scanning.

7. Turn the manual switch for the laser to reenable it.

8. Proceed with all steps in the Laser Alignment Section.

9. Once the laser is aligned it is time to make sure the tip is functioning properly. This process can be done by clicking the NCM ASetup button in the Scan control window. The AFM will automatically set parameters and attempt to get a frequency sweep of the NC-AFM tip. This can also be done by closing and reopening XEP while the machine is set up to do NC-AFM. This process can be repeated at any time as long as the tip is not within scanning range of a sample.

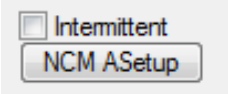

10. The NC-AFM setup will automatically open the frequency sweep from the NC-AFM (see figure B.7). Now that the laser is aligned, and assuming the tip is functioning properly, there will be a singular peak roughly 20 nm in height. If there is a secondary peak, the tip either has something like a dust particle attached to it, or is defective. If there is no peak check the laser alignment. Once verified the tip is ready for a scan, click done. This window can be reopened at any time by rerunning the NC-AFM setup or by going to settings then Frequency Sweep.

11. The AFM is now ready for an NC-AFM scan. Refer to the C-AFM and Taking a Scan section and the following extra details for specifics.

12. Additional Information: As opposed to C-AFM the gain is not the only tool for taking high quality scans. The Drive and Set Point can also be very useful especially on smooth samples. For example, if upon approach the signal from the NC-AFM is a large sine wave where the yellow and blue lines are opposite each other (obviously the AFM is not tracking) increasing the Drive by 5-20% can get the AFM to track. Variation of the Set Point should only be attempted after increasing the Drive, however varying it by $\pm$ 1 nm has proven useful to the author.

B.4 I-AFM

To change the AFM from C-AFM to I-AFM requires a change of tip, modification of the AFM head, the attachment of an external module, changes in the XEI software, and a laser realignment.

1. Proceed with all steps in the AFM Head Removal section.

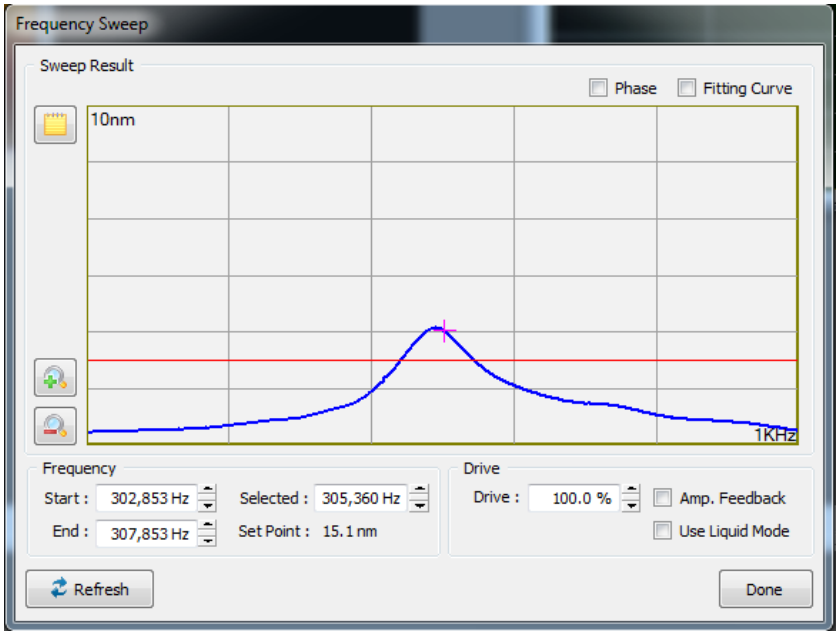

Figure B.7: Frequency sweep on NC-AFM tip

2. Open the wooden I-AFM box. You will need: STM/ I-AFM Frame Module, I-AFM Head Module, and the included VGA to 8 pin male DIN connector.

3. With a small phillips head screwdriver, remove the two panels from the AFM head seen in figure B.8.

4. Use tweezers to disconnect the CN4 cable. and replace the removed metal panel. This cable is normally used to send bias to the AFM tip and should be connected for C-AFM, NC-AFM, and EFM.

5. Attach the I-AFM Head module where the other panel, next to the AFM tip. Use a 1.5 mm alan wrench for these screws. Once assembled the head should look like figure B.8 without the I-AFM Tip attached.

6. Using tweezers, remove an I-AFM head and attach it magnetically, aligning the projections to the metal AFM tip holder as with NC-AFM and C-AFM tips. Carefully insert the wire into the I-AFM head module. The completed setup should look like the last image in figure B.8

7. Carefully replace the AFM head by sliding it from right to left along the rails until it stops. Move the plastic tabs backward to their original position and reattach the power cable to the side of the AFM head.

8. Put the STM/ I-AFM Frame Module into its holder on the left side of the AFM and attach the cable coming from the back of the AFM to the top of the module (labeled CBL-FRM2FRP-A). Attach the VGA port to the frame module (note the screws on

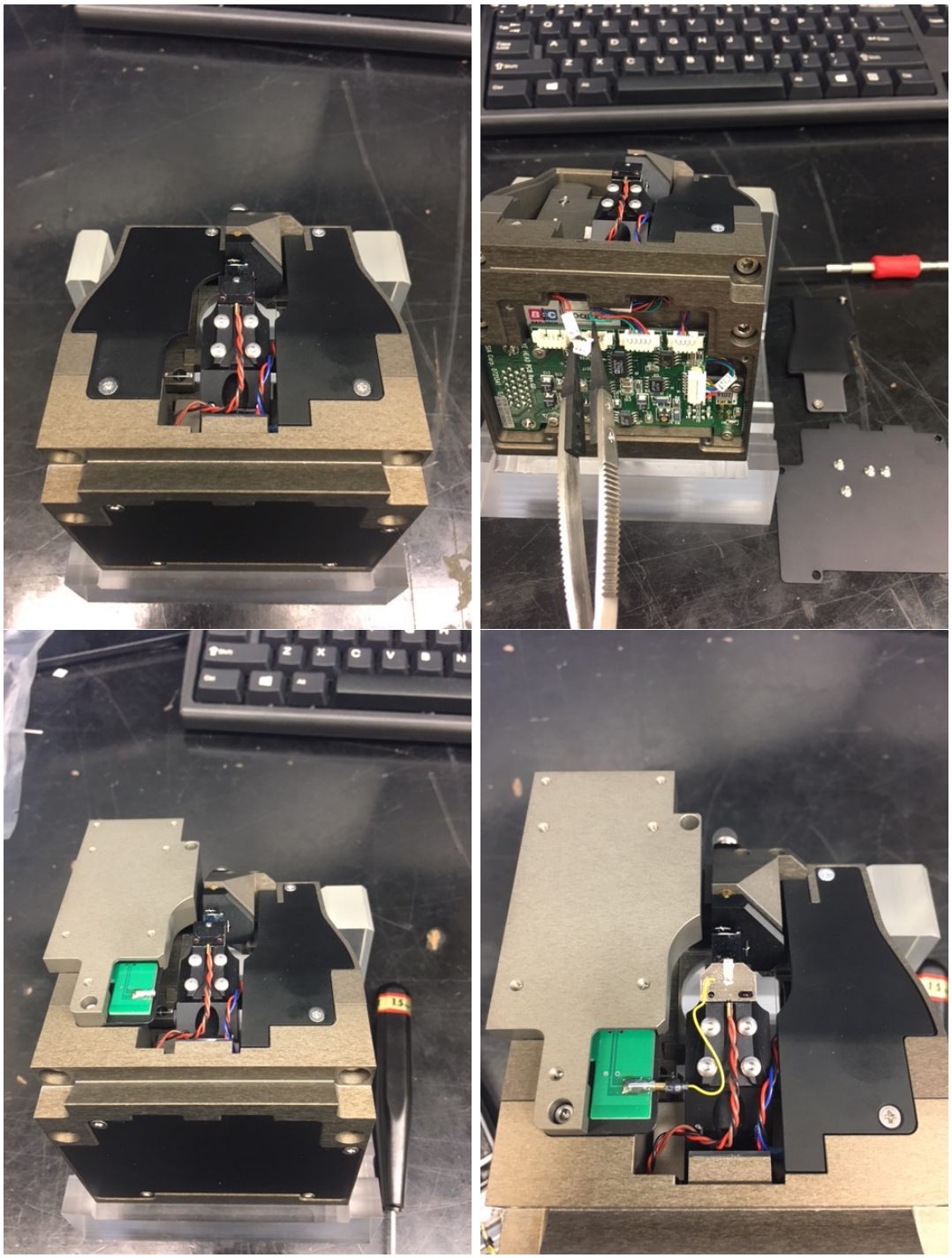

Figure B.8: I-AFM head assembly following steps 3-6.

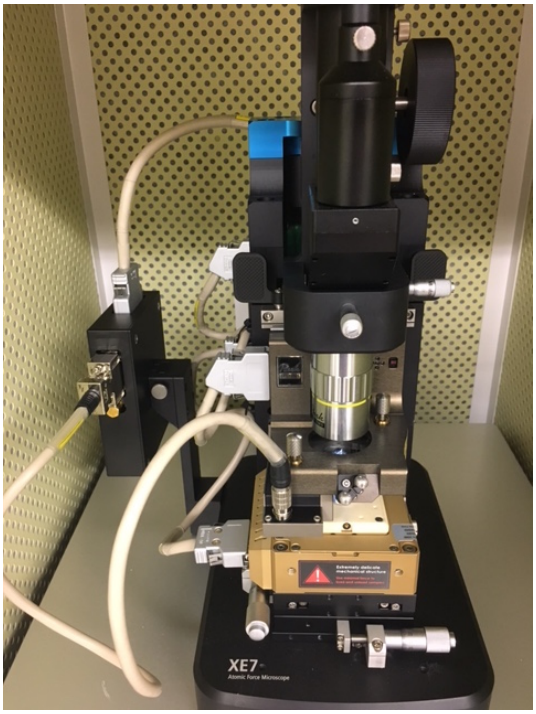

Figure B.9: I-AFM Assembly

this AFM are stubborn, just need to make sure the cable is held in place). Run this cable and attach the DIN side to the female port on the I-AFM Head Module. The finished assembly is shown in figure B.9.

9. Click on the drop down menu next to the icon used to turn the head off, set the system to I-AFM. The software will prompt you to make sure you wish to change the mode of the head (see figure B.6).

10. Now go to Setup, then Part Config. Open the dropdown menu next to Cantilever. This will show all AFM tip types known to the XE7 Software. Look at the box from which the I-AFM tip came from. On the label will be an identifier called Item. This is the type of tip in the box. Find this in the dropdown menu and select it. Note: the item names will not match perfectly since they will sometimes have identifying letters in front or at the end of the name of the tip such as PPP, 5M, 10M, etc.

11. Once you are sure you have told the system what mode it should be in and what tip is installed, turn the head back on.

12. Turn the manual switch for the laser to reenable it.

13. Proceed with all steps in the Laser Alignment Section.

14. Go to Setup then Input Config (see figure B.10). For most scans done in I-AFM mode, choose to show Topography, Error Signal, Current, and Log Current.

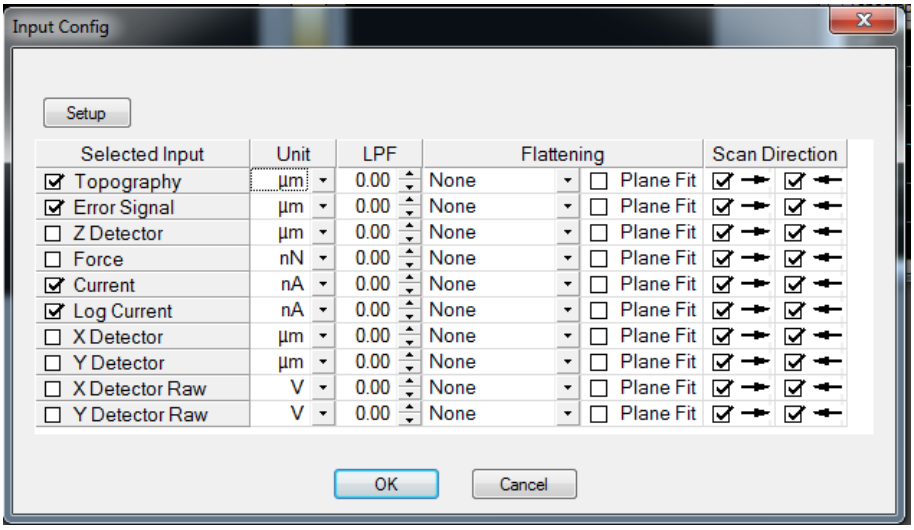

Figure B.10: I-AFM Input Config

15. To view these new input readouts, go to View, then Show Trace Control Window. Then set the control window to whatever parameter necessary to monitor (usually current).

16. The AFM is now ready for an I-AFM scan. Refer to the C-AFM and Taking a Scan section and the following extra details for specifics.

17. Additional Information: Once a successful scan has been taken the I-AFM will now have a topographical reference for isolated IV curves. To change the I-AFM into this mode either select the icon or go to Mode then I/V Spectroscopy. The I-AFM will stop scanning at this point. Right click on any spot on any of the images and select Move Here to move the I-AFM tip automatically to that point. IV curves can now be taken based on applied specifications. To export the data right click the IV curve and copy to clipboard. Paste in some form of text editor. Note: In the authors experience limiting the current is a hard limit for the scan, limiting the Voltage is not as reliable.

B.5 SCM

To change the AFM from C-AFM to SCM requires a change of tip, a modification of the AFM head, the attachment of an external module, changes in wiring to include the Lock-In Amplifier, changes in the XEI software, and a laser realignment.

1. Proceed with all steps in the AFM Head Removal section, however **put the head assemble at max height of 29000 μm. There are a lot of components for this mode and you need the space!**

2. Open the wooden SCM box. You will need: SCM Probe Hand, two cables with brass heads on both ends, SCM Resonator, SCM Frame Module, SCM Sample Holder.

3. With a small phillips head screwdriver, remove the two panels from the AFM head seen in figure B.11.

4. Use tweezers to disconnect the CN4 cable and fully pull it out of the front of the AFM head. This cable is normally used to send bias to the AFM tip and should be connected for C-AFM, NC-AFM, and EFM. In the case of SCM the entire head assembly must be removed since SCM needs a non-conductive and non-magnetic tip holder and has it's own CN4 cable.

5. Remove the AFM Probe and and replace it with the SCM Probe Hand. This is done by removing the four screws with a 1.27 mm allan wrench and using them to attach the SCM Probe Hand. Feed the attached wire though and attach it to the CN4 slot (see figure B.11). This is best done with the help of tweezers.

6. Replace the back panel covering the CN4 cable and circuit board.

7. Where the other panel, located by the AFM head, attach the SCM Resonator using the screws from the removed panel and a small phillips screwdriver (see figure B.11).

8. Insert the SCM Probe into the SCM Probe Hand and insert the wire into the SCM resonator (see figure B.11). Push down on the plastic arm for insertion of the SCM tip and align the holes in the tip with the raised red bumps on the SCM Probe Hand. This is a delicate process so plan out movements and take the appropriate amount of time.

9. Replace the Sample stage with the SCM Sample Holder by simply unscrewing and replacing it (the SCM stage is taller.

10. Carefully replace the AFM head by sliding it from right to left along the rails until it stops. Move the plastic tabs backward to their original position and reattach the power cable to the side of the AFM head.

11. Put the SCM Frame Module into its holder on the left side of the AFM and attach the cable coming from the back of the AFM to the top of the module (labeled CBL-FRM2FRP-A). Using the two cables connect the SCM Resonator to the SCM Frame Module (they are labeled DTCTR and RFOUT on both modules). The finished assembly is shown in figure B.12 although the only difference will be the cable coming from the Lock-In Amplifier shown in the following steps.

12. To wire the lock in Amplifier into the loop wiring changes need to be made. How to do this is best described by figure B.13. Generally though the following steps need to be followed:

    - Attach CH1 Output on the front of the Lock in Amplifier to AUX ADC1 on the back of the XE-Series SPM Controller.
    - Attach CH2 Output on the front of the Lock in Amplifier to AUX ADC2 on the back of the XE-Series SPM Controller.

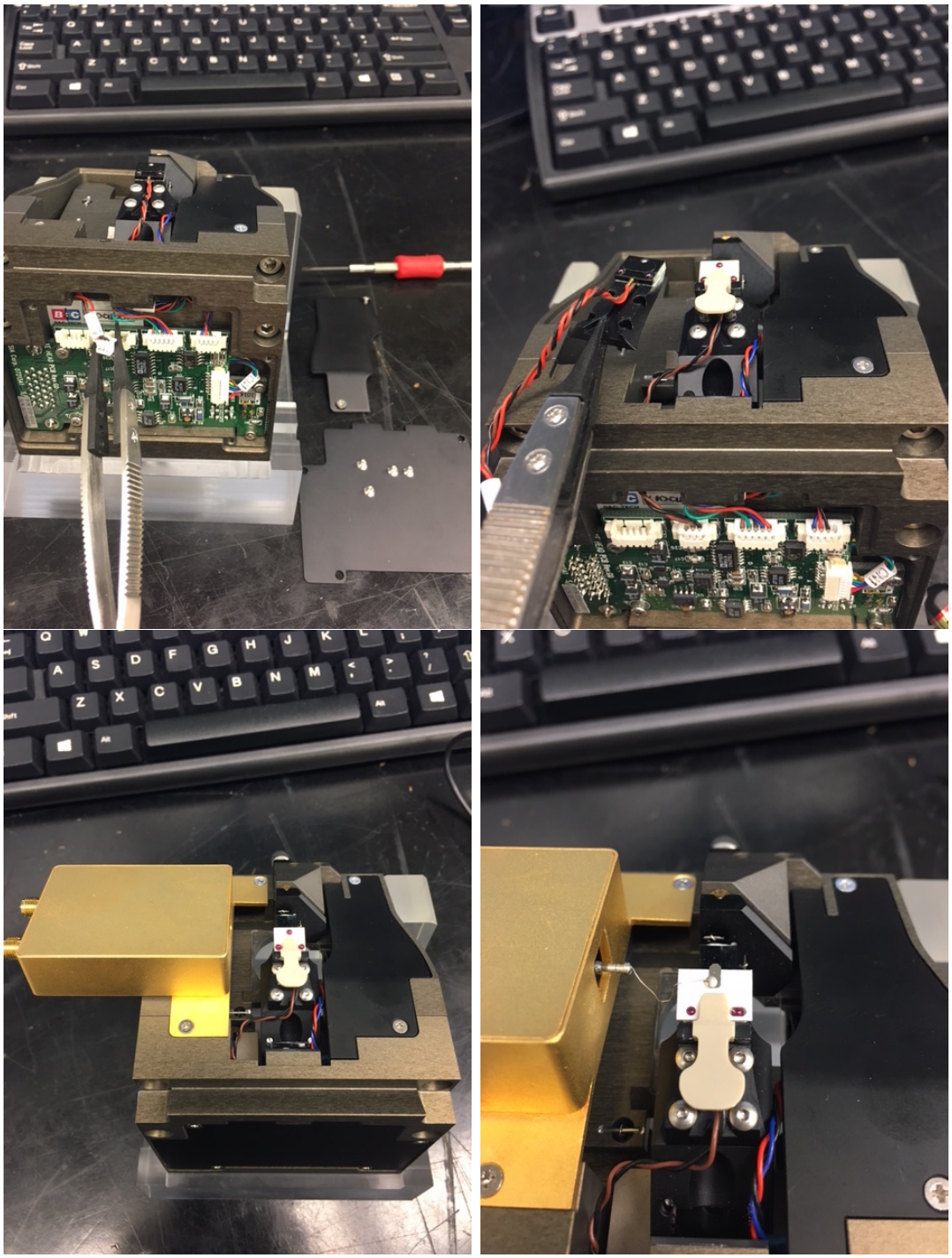

Figure B.11: SCM head assembly following steps 3-7.

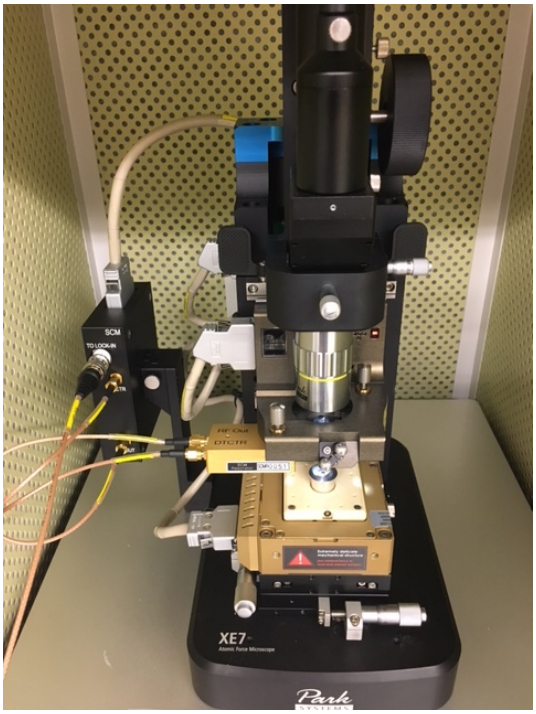

Figure B.12: SCM Completed Assembly

- Attach Sine Out on the front of the Lock in Amplifier to EXT. bias Sample on the back of the XE-Series SPM Controller.
- Attach A/I on the front of the Lock in Amplifier to TO LOCK-IN on the front of the SCM Frame Module.

13. Click on the drop down menu next to the icon used to turn the head off, set the system to SCM. The software will prompt you to make sure you wish to change the mode of the head (see figure B.6).

14. Now go to Setup, then Part Config. Open the dropdown menu next to Cantilever. This will show all AFM tip types known to the XE7 Software. Look at the box from

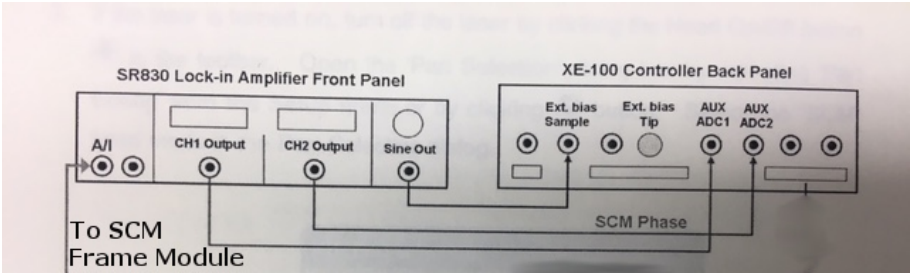

Figure B.13: SCM Wiring from ([9] p.15)

which the SCM tip came from. On the label will be an identifier called Item. This is the type of tip in the box. Find this in the dropdown menu and select it. Note: the item names will not match perfectly since they will sometimes have identifying letters in front or at the end of the name of the tip such as PPP, 5M, 10M, etc.

15. Once you are sure you have told the system what mode it should be in and what tip is installed, turn the head back on.

16. Turn on the Lock-In Amplifier (power switch on back).

17. Turn the manual switch for the laser to reenable it.

18. Proceed with all steps in the Laser Alignment Section.

19. Go to Setup then Input Config which is the same as the I-AFM input options, but current is replaced with SCM Detector (see figure B.10). Choose whatever the scan requires to be tracked.

20. To view these new input readouts, go to View, then Show Trace Control Window. Then set the control window to whatever parameter necessary to monitor (usually current).

21. The AFM is now ready for a SCM scan. Refer to the C-AFM and Taking a Scan section or the SCM manual [9] for specifics.

B.6 EFM

To change the AFM from C-AFM to EFM requires a change of tip, changes in wiring and the addition of an attenuator, changes in the XEI software, and a laser realignment.

1. To change the AFM from C-AFM to EFM, proceed through all steps in the AFM Head Removal section. Then refer to the NC-AFM section steps 2-7 but install the EFM tip since the process is the same, however, no frequency sweep window will pop up in step 6. Finally proceed through all steps in the Laser Alignment section. This will set up the AFM to run in EFM.

2. For EXT-EFM, or EFM that uses the external lock in amplifier additional wiring is needed. Additonally in the drop down menu select EFM(EXT) instead of EFM. Figure B.14 explains this process however the following steps should be followed:

    - Connect CH1 Output on the front of the Lock-In Amplifier to Aux1 on the back of the XE-Series SPM Controller.
    - Connect CH2 Output on the front of the Lock-In Amplifier to Aux2 on the back of the XE-Series SPM Controller.
    - Connect Sine Out on the front of the Lock-In Amplifier to ext. Tip Bias on the back of the XE-Series SPM Controller.

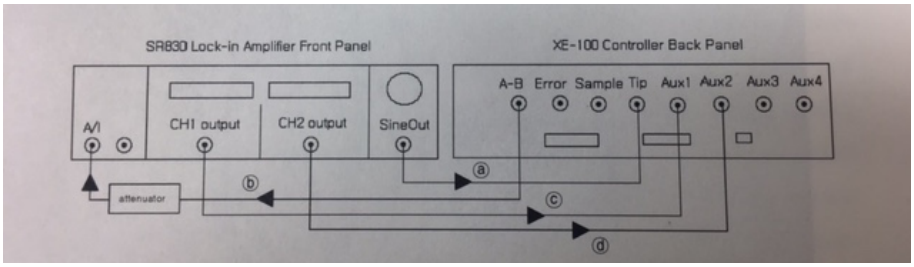

Figure B.14: EXT-EFM Wiring from ([1] p.10)

- Connect A-B on the back of the XE-Series SPM to the in on the Park Systems 1/10 Attenuator IN port then attach a cable from OUT on the Attenuator to A/I on the front of the Lock-In Amplifier.

3. Turn on the Lock-In Amplifier and proceed with scans. Refer to the C-AFM and Taking a Scan section or the EFM manual [1] for specifics.

B.7 AFM Head Removal

1. Begin by making sure the optical microscope is raised above the head assembly of the microscope and that the head is also high enough to comfortably access and remove the entire head assembly. Press the Lift Z button to raise the stage (see figure B.3). Generally having the z stage at a height of 10000 μm is enough (this does not apply to SCM as the assembly should be raised significantly higher). Remove any samples from the system.

2. For safety disable the laser manually by using the red switch (or beam switch) on the head of the microscope (see fig. B.1). You will know it has been disabled from the red led of the switch turning off, the Beam Position Indicator LED's will turn off, and the PSPD in the XEP software will no longer show a red dot. The laser will be off when you perform the next step (turning off the AFM head), so this is not necessary, but as a safety precaution it can not hurt.

3. Turn off the AFM head. This is done in the XEP software by clicking the AFM Head icon. The icon is located in the upper left corner of the XEP GUI. The program will prompt you asking if you really want to turn the head off.

4. Remove the power cable from the side of the AFM head by pinching the metal tabs on the side (see figure B.15).

5. Move the two black plastic wings on either side of the microscope forward. This will unlock the head and allow it to slide on the rails for head removal (see figure B.16.

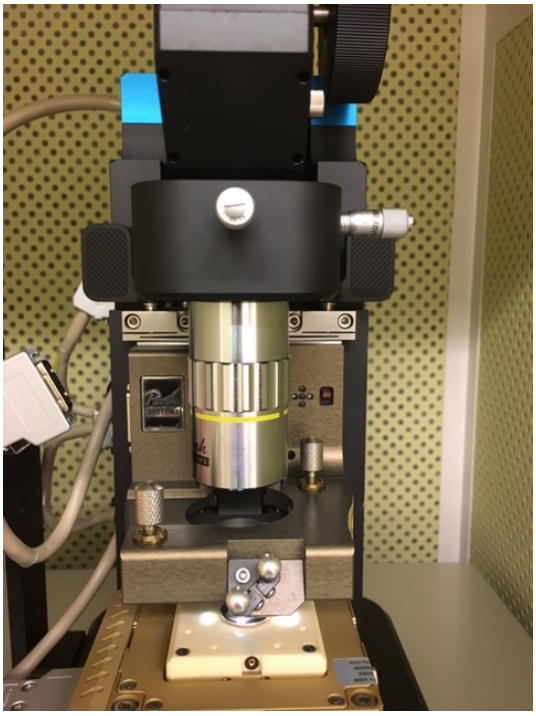

Figure B.15: Removal of Power Cable from AFM head

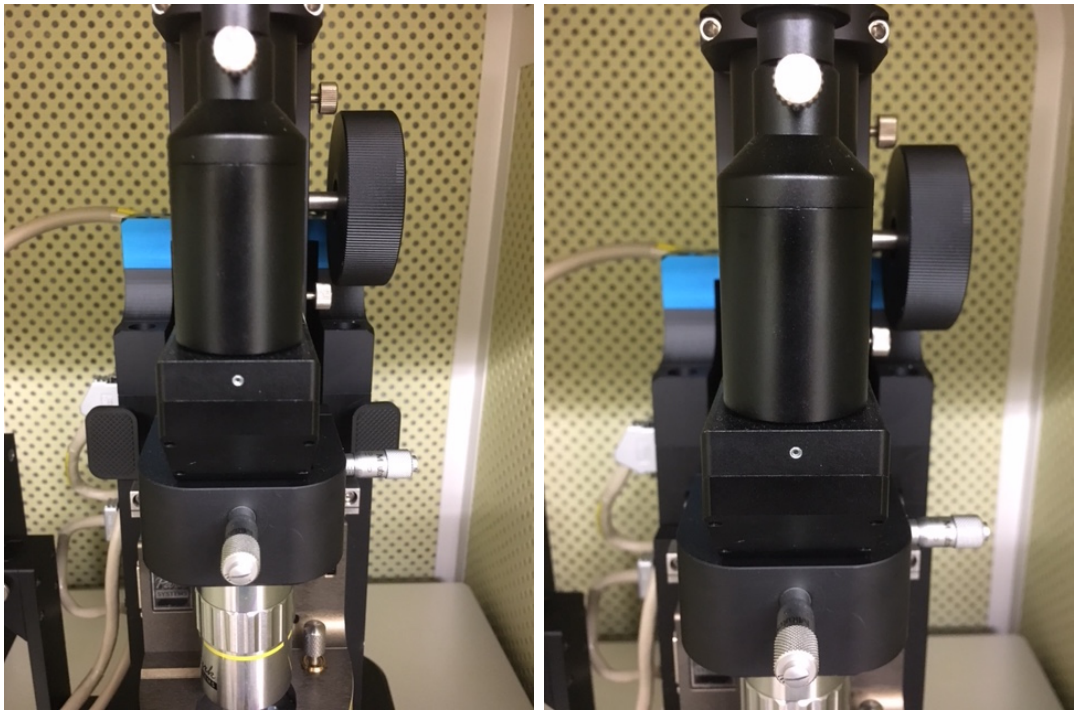

Figure B.16: Flaps for unlocking AFM head for removal

6. Carefully slide the AFM head out of the microscope by grasping the sides firmly and sliding it from left to right. Once removed flip it upside down so that the AFM tip is visible and place it in the clear plastic holder.

B.8 Laser Alignment

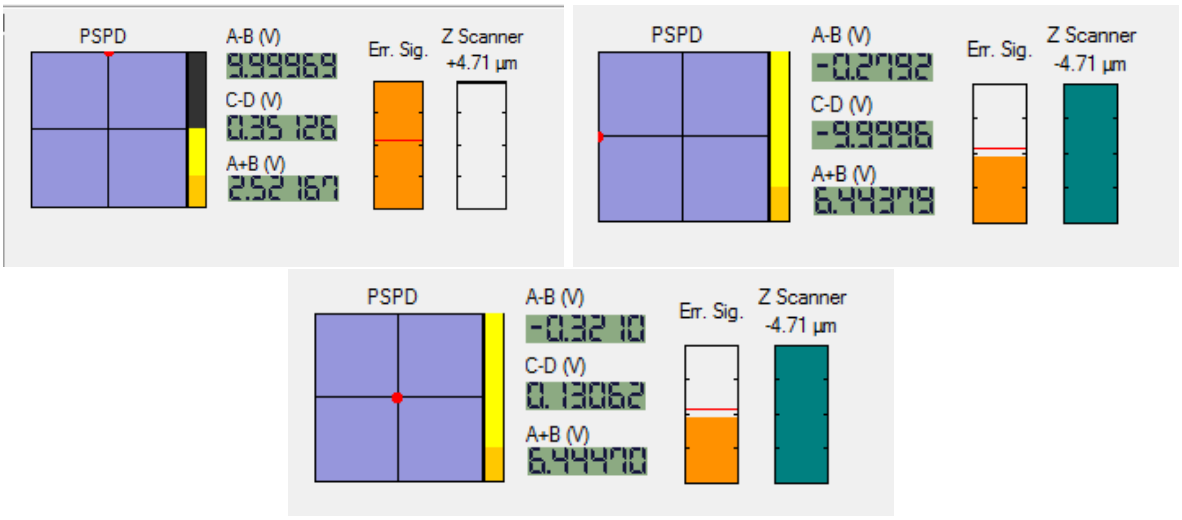

Figure B.17: Steps for Aligning Laser using Steering Mirror Adjusting Screws

1. Begin by using the focus knob (large black circular knob on right side of ocular microscope) to focus on the AFM tip.

2. Use the Illuminator slider, located above the error log in XEP, to 0%. This slider controls the light from the optical microscope. Turning this light off will allow the laser reflecting off the back of the AFM tip to be seen.

3. Using the beam alignment screws (see figure B.1) move the laser onto the lower portion of the tip (see figure B.18). The red circle in this figure indicates roughly where the center of the laser dot should be, however, this does not need to be perfect. If there is trouble finding the laser dot putting a white piece of paper on the stage will reduce reflection and make the dot more visible. Careful when removing the paper as it is very likely, since the paper can bend upwards, that the paper will crash into and break the AFM tip.

4. Now use the steering mirror adjusting screws (see figure B.1) to align the reflected laser with the ccd (see figure B.17). To do this efficiently, first only turn one of the screws. If the intensity, represented by the yellow bar on the side of the PSPD, decreases turn the screw the other way. Turn the screw until you see movement of the red dot. Put the red dot near the center line on whichever side it is on. Next, turn the other screw using the same method and align it with the center, depending on how aligned it was

initially you may not need to do this step. Once the dot moves off the side of the PSPD slowly turn the screws on at a time until the dot is centered in the crosshair. The A-B value (lateral) and C-D value (vertical) should be as close to 0 as possible. At any time during a scan they should stay within -2 to 2 volts. This alignment can be, and should be, done at any time as long as the tip is not in contact with a sample. The A+B is related to the intensity of the spot, also represented by the yellow bar, and should be maximized. A minimum would be 2 volts, however, with most tips used by the author show values above 5.5 volts.

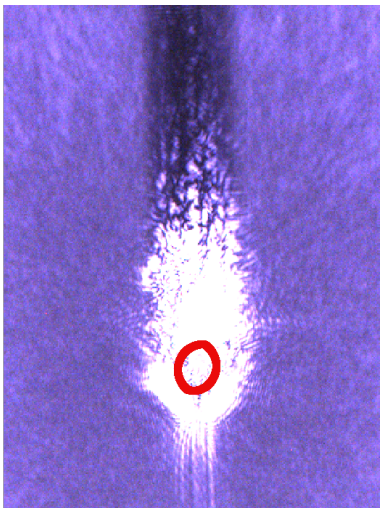

Figure B.18: Laser Dot centered